

**MASTER**

**Multiscale Modelling of Transient Absorption in Disordered Organic Molecular Systems**

Gerritsen, R.H.J.

*Award date:*  
2020

[Link to publication](#)

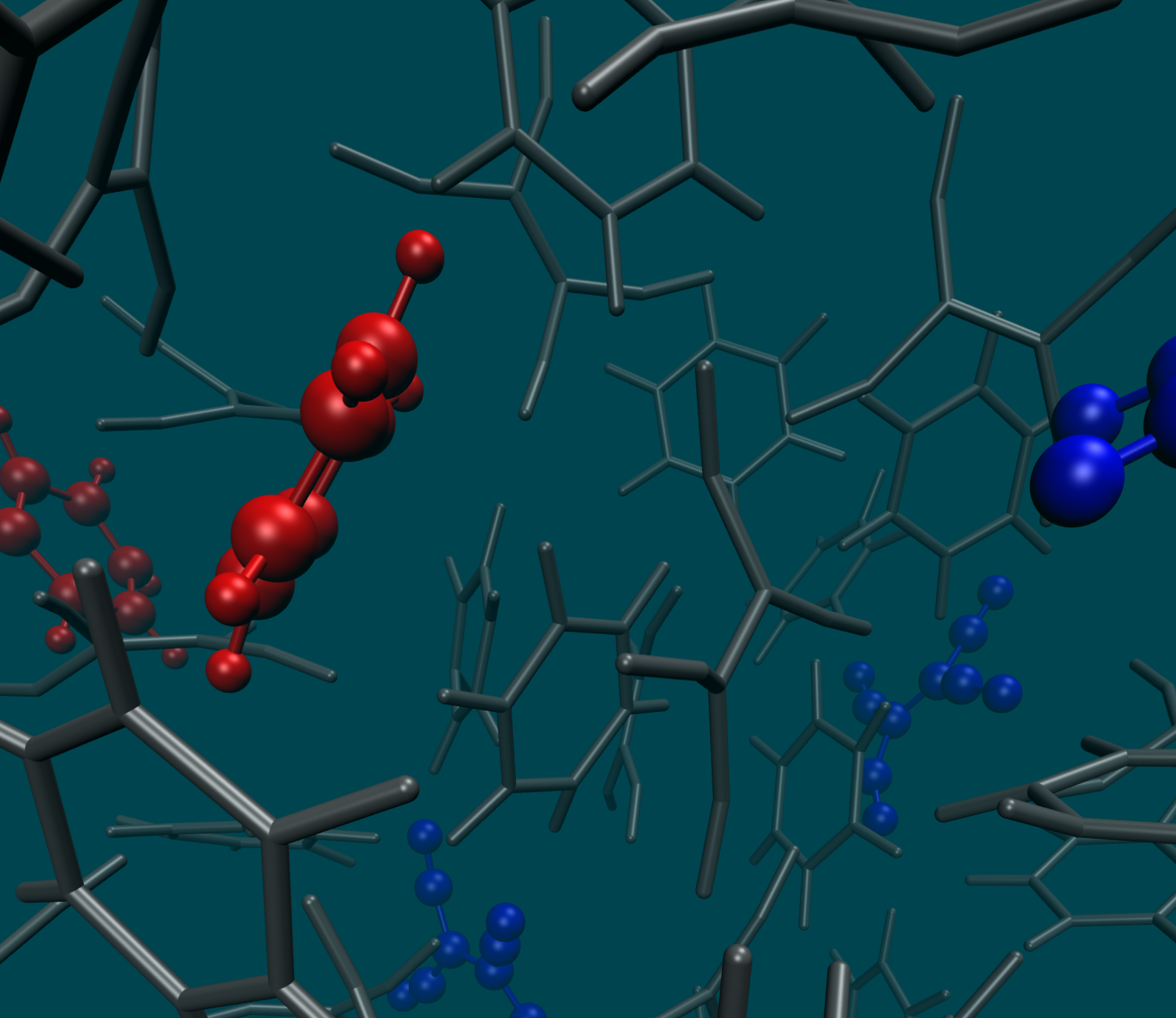
**Disclaimer**

This document contains a student thesis (bachelor's or master's), as authored by a student at Eindhoven University of Technology. Student theses are made available in the TU/e repository upon obtaining the required degree. The grade received is not published on the document as presented in the repository. The required complexity or quality of research of student theses may vary by program, and the required minimum study period may vary in duration.

**General rights**

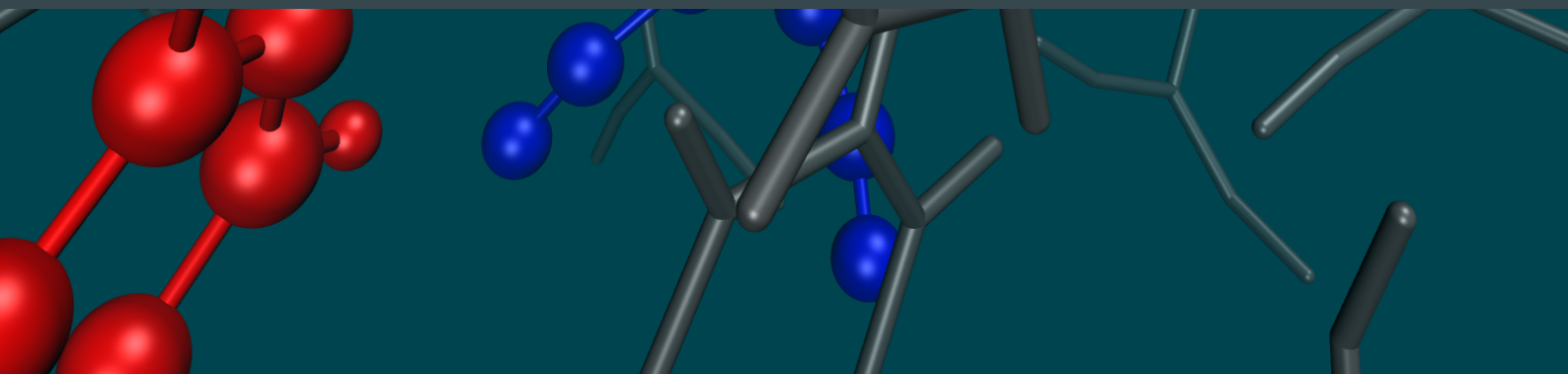
Copyright and moral rights for the publications made accessible in the public portal are retained by the authors and/or other copyright owners and it is a condition of accessing publications that users recognise and abide by the legal requirements associated with these rights.

- Users may download and print one copy of any publication from the public portal for the purpose of private study or research.
- You may not further distribute the material or use it for any profit-making activity or commercial gain



# Multiscale Modelling of Transient Absorption in Disordered Organic Molecular Systems

Ruben Gerritsen



**Ruben Gerritsen**

*Multiscale Modelling of Transient Absorption in Disordered Organic Molecular Systems*

Master thesis, July 6, 2020

Front cover: artist impression of a benzene TCNE mixture generated with VMD [1].

Supervisor and tutor: dr. Björn Baumeier

Assessment committee: dr. Björn Baumeier, Prof.dr.ir. Barry Koren and Prof.dr. Remco van der Hofstad

**Eindhoven University of Technology**

Department of Mathematics and Computer Science

Baumeier Research Group

## **Abstract**

The most important processes in organic electronics are charge and exciton dynamics. These processes are ultrafast, in the femto- to picoseconds range. This makes the processes almost impossible to measure in an experiment. Transient Absorption Spectroscopy (TAS) is one of the few techniques that give some information about the ultrafast dynamics. There is, however, difficulty in the interpretation of the resulting transient absorption spectra. This thesis discusses a multiscale model that can assist in the interpretation of these spectra. A kinetic Monte Carlo (KMC) approach is used to model the dynamics of the system and it is parametrized using state-of-the-art quantum-mechanical calculations, such as the DFT-GW-BSE method. The same quantum-mechanical calculations are used to obtain the optical absorption spectra of the molecules. The state of the KMC simulation is then linked to the absorption spectra of the molecules to simulate the TAS signal. Features of the simulated TAS signal can subsequently be linked to the underlying dynamics.

# Contents

<b>Abstract</b>	<b>i</b>
<b>1 Introduction</b>	<b>1</b>
1.1 A Very Short Introduction to Organic Electronics . . . . .	1
1.1.1 Charge Transport . . . . .	3
1.1.2 Spectroscopy . . . . .	4
1.1.3 Processes in Organic Electronics . . . . .	5
1.2 Transient Absorption Spectroscopy . . . . .	5
1.3 Multiscale Modelling Approach . . . . .	6
1.4 Scope and Layout of the Thesis . . . . .	7
<b>2 Many-Body Theory of Molecular Systems</b>	<b>8</b>
2.1 Many-Electron Systems . . . . .	8
2.1.1 The Born-Oppenheimer Approximation . . . . .	9
2.1.2 The Wavefunction and the Variational Principle . . . . .	10
2.1.3 Non-interacting Electrons . . . . .	12
2.1.4 The Hartree-Fock Approximation . . . . .	12
2.1.5 Solving the Hartree-Fock equation . . . . .	13
2.1.6 Basis sets . . . . .	14
2.1.7 Limitations of the Hartree-Fock Approach . . . . .	15
2.2 Density Functional Theory . . . . .	15
2.2.1 The Hohenberg-Kohn Theorems . . . . .	16
2.2.2 The Kohn-Sham Equations . . . . .	18
2.2.3 Exchange-Correlation Functionals . . . . .	19
2.3 Excited States via <i>GW</i> -BSE . . . . .	20
2.3.1 Single Particle Excitations, the <i>GW</i> Method . . . . .	21
2.3.2 Two Particle Excitations, the Bethe Salpeter Equation . . . . .	22
2.3.3 Optical Spectra . . . . .	23
2.4 Excited States via TDDFT . . . . .	24
2.4.1 Runge-Gross Theorem and Time-Dependent Kohn Sham Equations . . . . .	24
2.4.2 Excitations . . . . .	24
<b>3 Exciton and Charge Carrier Dynamics in Disordered Organic Molecular Systems</b>	<b>26</b>
3.1 The Hopping Model . . . . .	26
3.1.1 The Master Equation . . . . .	27
3.1.2 The Master Equation for a Single Carrier . . . . .	27
3.1.3 The Master Equation for Multiple Carriers . . . . .	27
3.2 Extending the Hopping Model . . . . .	28
3.2.1 Charge Transfer . . . . .	29
3.2.2 Exciton Transfer . . . . .	29
3.2.3 Exciton Generation . . . . .	29

---

3.2.4	Exciton Dissociation . . . . .	30
3.2.5	Exciton Decay . . . . .	30
3.2.6	The Kinetic Monte Carlo Algorithm . . . . .	30
3.3	Material Morphology and Rate Parameter Calculations . . . . .	31
3.3.1	Site Locations and Simulation Box . . . . .	31
3.3.2	Site Energies . . . . .	31
3.3.3	Reorganization Energies . . . . .	31
3.3.4	Electronic Coupling Elements . . . . .	32
3.3.5	Attempt Frequency and Localization Length . . . . .	32
<b>4</b>	<b>Transient Absorption of a Benzene TCNE Mixture</b>	<b>33</b>
4.1	The Model System . . . . .	33
4.1.1	Computational Methods and Simulation Method . . . . .	33
4.1.2	The Density Of States . . . . .	34
4.1.3	Processes Visualized . . . . .	36
4.1.4	Rates . . . . .	36
4.1.5	Accuracy, Performance and Sensitivity of the Methods . . . . .	39
4.2	Simulating the Transient Absorption Spectrum . . . . .	41
4.2.1	Carrier Dynamics . . . . .	41
4.2.2	Transient Absorption Spectrum . . . . .	41
4.3	Simulating Different Cases . . . . .	43
4.3.1	Reduced Charge Transfer State Binding Energy . . . . .	43
4.3.2	Reduced Gap Between Donor and Acceptor . . . . .	43
4.3.3	All Singlets . . . . .	43
<b>5</b>	<b>Conclusion and Future Work</b>	<b>48</b>
5.1	Conclusions . . . . .	48
5.2	Future Work . . . . .	48
5.2.1	Improving the Model . . . . .	48
5.2.2	Different Approaches to Carrier Dynamics . . . . .	49
<b>A</b>	<b>Computation of Transition Dipoles</b>	<b>51</b>
<b>B</b>	<b>The Master Equation Extras</b>	<b>55</b>
	<b>Bibliography</b>	<b>57</b>
	<b>Acknowledgements</b>	<b>62</b>

# Chapter 1

## Introduction

The field of organic electronics has seen some major advancements over the last few years. Almost all current flagship phones have organic light emitting diode (OLED) displays [2] and the first foldable phones are based on the same technology. Other fields of organic electronics like organic solar cells are less developed but may provide a cheaper alternative to their inorganic counterparts and are easier to process [3]. To unlock the true potential of the whole field of organic electronics, a thorough understanding is needed of the physical processes that underlie organic electronic devices.

The most important processes in organic electronic devices are charge and energy transport [4, 5]. These processes occur at a time scale in the order of pico- and femtoseconds. A timescale so small that most experimental techniques fail to identify the exact dynamics that occur. Nonetheless there are experimental techniques that can be used to get an indirect measurement of the processes. One of these techniques is Transient Absorption Spectroscopy (TAS) also known as pump-probe spectroscopy.

The main challenge of TAS is that dynamics are not observed directly, but can only be inferred from the absorption spectra. It is particularly difficult to assign the spectral features of the absorption spectra unambiguously to the underlying dynamic processes. The aim of this thesis is to provide a mathematical model that can assist in inferring dynamical processes from transient absorption spectra. The dynamical processes depend both on the material morphology (i.e. the layout of the molecules in the material) and the quantum mechanical electronic structure of the individual molecules. A multiscale modelling approach is therefore required.

In this first chapter we will introduce the basic ideas of organic electronics and spectroscopy. Then we give an overview of the multiscale model needed to describe the dynamics and corresponding absorption spectra. Finally we present the scope and layout of this thesis.

### 1.1 A Very Short Introduction to Organic Electronics

Organic materials are built up from organic molecules, i.e. they are mostly made up of carbon and hydrogen atoms. The atoms are bound together by the electrostatic force between the positive nuclei of the atoms and their negatively charged electrons. The electrons are in constant movement, they fly in between and around the nuclei of the molecule. Since the molecules, nuclei and electrons are extremely small, classical mechanics fails at describing the molecules and quantum mechanics is needed. In quantum mechanics the electrons cannot attain any arbitrary amount of energy, but only discrete energy levels. Every energy level has a region in space associated with it, where it is most likely to find the corresponding electron. The energy level and the region in space are bundled in the concept of *orbitals*. Each molecule has different orbitals associated with it that can be occupied by two electrons of opposite spin. The full concept and the details of orbitals will be explained in Chapter 2.

In the ground state of a molecule,  $S_0$ , the lowest energy orbitals of the molecules are occupied and the higher orbitals are empty, the energy of this state is denoted by  $E_0$ . The energy difference between the highest occupied molecular orbital (HOMO) and lowest unoccupied molecular orbital

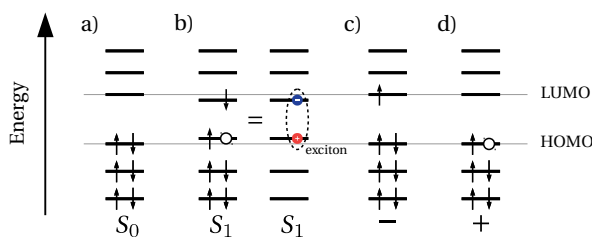


Figure 1.1: Energy diagrams of a) the ground state, b) an exciton, where we have drawn the energy levels closer together to indicate that we should not forget about the associated binding energy, c) an anion (negatively charged excitation), d) a cation (positively charged excitation).

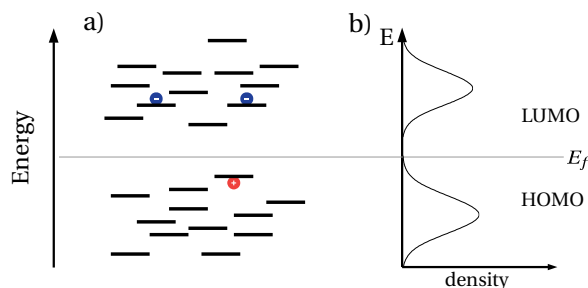


Figure 1.2: a) The LUMO and HOMO levels in a disordered organic material, due to their interaction every level is shifted a bit. The grey line indicates the Fermi level and is added as a visual aid to distinguish the HOMO and LUMO levels. Also some free charges have been added. b) the density of states (DOS) corresponding to Figure a.

(LUMO) is called the electronic (band)gap energy  $E_g$ . The different orbitals are often drawn in an energy diagram (see Figure 1.1a) where every orbital is indicated by a line and arrows are used to indicate the occupation of a level by a spin up or down electron.

Besides the ground state there are infinitely many other states of the molecule that we call excited states. In general we can classify them as neutral or charged. In a neutral excited state an electron is promoted, for example through the absorption of a photon (i.e. light), from an occupied orbital to one of the unoccupied orbitals. To simplify the picture we call the absence of an electron a hole. A neutral excited state (exciton) can then be thought of as an electron hole pair, see Figure 1.1b. Since the hole is positively charged and the electron negatively they attract via the Coulomb interaction. Also there are (spin dependent) quantum mechanical interactions between the electron and hole. These interactions lead to an exciton binding energy which is the energy difference between the electron and the hole separately on two molecules infinitely far apart and the energy for the hole and electron on the same molecule. Due to this binding energy the exciton behaves as one particle. Energies of excited states  $\Omega_i$  are given relative to the ground state energy, e.g. for the first excited state  $S_1$  with energy  $E_1$  we have

$$\Omega_1 = E_1 - E_0. \quad (1.1)$$

Excitons come in two flavours, singlets and triplets, depending on their spin configuration. For molecules with an even number of electrons only singlets are optically active (i.e. absorb a photon on creation and emit a photon on decay) and are of main interest in this thesis. The terms excitons and singlets will therefore be used interchangeably unless explicitly stated otherwise. Charged excited states occur if the net charge on a molecule is not zero. For example we could have an extra electron or an extra hole (absence of an electron) present on the molecule, see Figure 1.1c)&d).

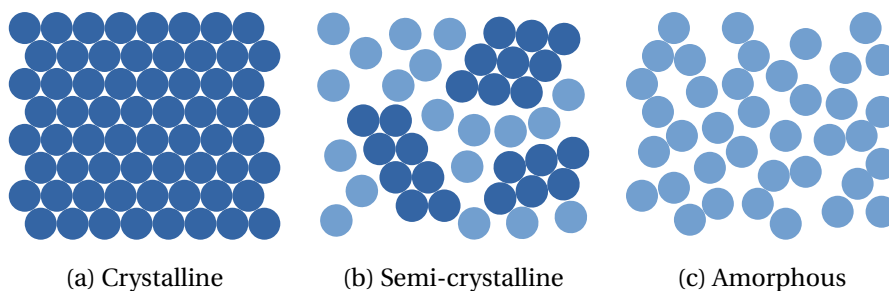


Figure 1.3: Different types of order and disorder in organic materials.

Materials are made up from many molecules that interact and polarize one another. This leads to shifts in the energy levels of the molecules. When we for example look at the HOMO and LUMO levels in an organic material we see that the energy levels for the individual molecules are shifted, see Figure 1.2a. This shifting is referred to as disorder in the density of states (DOS). The density of states is literally the density of the number of available states at a certain energy. Since there are a lot of molecules in a material (in the order of  $10^{23}$ ) the law of large numbers applies and we see that the density of states approximately forms a Gaussian distribution for the different energy levels, Figure 1.2b.

### 1.1.1 Charge Transport

The molecules in a organic material can have different spatial arrangements depending on the molecules and the processing technique used. The material can either be highly ordered (crystalline), highly disordered (amorphous) or a combination of both with ordered and disordered regions (semi-crystalline), see Figure 1.3. The spatial arrangement of the molecules determines the type of charge transport that can occur. In crystalline materials the different electronic states of the molecules combine to form bands that stretch large parts of the material and electrons and holes can move more or less freely within the band. This type of transport is called band-like transport because it resembles the band transport in inorganic semiconductors. In highly disordered materials, electronic states do not combine (overlap) and every molecule has its own electronic states. This leads to localization of charges in a disordered organic material, i.e. the charges are confined to some space (a molecule or part of it) that we call a site. Since charges are confined to sites they cannot move around freely and charge transport does not occur band-like. Instead it occurs as a quantum mechanical tunnelling process, which can be thought of as charges hopping from one site to another, this type of transport is often called phonon (i.e. temperature) activated hopping [6]. In semi-crystalline materials combinations of the two types of transport occur, in the crystalline regions electrons move band-like and in the disordered regions they need to hop. In this thesis we are concerned with disordered organic materials, and hence, are interested in hopping transport.

To describe hopping transport, hopping models are used. A hopping model consists of *sites* and *hopping rates*, see Figure 1.4. The hopping rates correspond to the probability that the charge carrier will hop from one site to another. Mathematically we can think of the system as a graph where the nodes represent sites and weighted edges represent the hopping rates.

Two often used rates are the Miller-Abrahams and Marcus rates, we will discuss them in more detail in Chapter 3. The Miller-Abrahams rate for a hop from site  $i$  to site  $j$  is given by

$$v_{ij} = \begin{cases} v_0 \exp\left(-2\alpha R_{ij} - \frac{\Delta E}{k_B T}\right) & \Delta E > 0 \\ v_0 \exp(-2\alpha R_{ij}) & \Delta E \leq 0 \end{cases}, \quad (1.2)$$

and shows us the main parameters for hopping transport. There is an attempt frequency  $\nu_0$  that

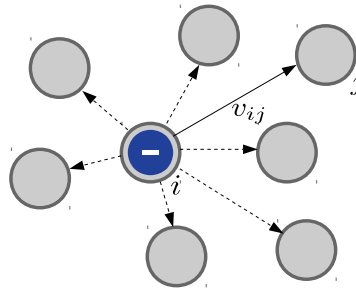


Figure 1.4: An illustration of the hopping model, grey circles represent sites, possible hops are indicated with arrows and for the hop from  $i$  to  $j$  the rate is given.

indicates the number of attempts to hop per time unit. There is an exponential term,  $\exp(-2\alpha R_{ij})$ , that penalizes the distance,  $R_{ij}$ , a charge needs to hop (large distances are less frequent). Finally there is a Boltzmann term,  $\exp\left(-\frac{\Delta E}{k_B T}\right)$ , where  $\Delta E$  is the energy difference between site  $i$  and  $j$  ( $\Delta E = E_j - E_i$ ). It describes the probability of absorbing a phonon (i.e. thermal energy) with enough energy to make the hop to a higher energy site and can be seen as a penalty for jumping to higher energy sites.

### 1.1.2 Spectroscopy

Transitions between states of a molecule do not occur out of the blue. A transition to a higher energy state needs energy and the transition to a lower energy state releases energy. This energy can be released or obtained from a phonon, photon or other energy source. Spectroscopy concerns itself with transitions between states due to photon (light) absorption or emission. A molecule in state  $i$  with energy  $E_i$  can transition into a higher energy state  $f$  with energy  $E_f$  via photon absorption if

$$E_f - E_i = h\nu \quad (1.3)$$

where  $h$  is the Planck constant and  $\nu$  the frequency of the photon. Besides the photon energy that needs to match the energy gap between the states, the photon also needs to be able to interact with the molecule. The amount of interaction is given by a transition dipole  $\boldsymbol{\mu}$ . In this thesis we will mostly be concerned with electric transition dipole moments

$$\boldsymbol{\mu} = \langle \Psi_f | \hat{\mathbf{r}} | \Psi_i \rangle \quad (1.4)$$

where the  $\Psi$ s are functions describing the initial state,  $i$ , and final state,  $f$ , of the molecule and  $\hat{\mathbf{r}}$  is an operator that gives the electric transition dipole.<sup>1</sup> The transition probability between two states is proportional to the square of the transition dipole moment. If we normalize this square with the excitation energy we arrive at the oscillator strength

$$f = \frac{2}{3} \boldsymbol{\mu}^2 \Omega_S. \quad (1.5)$$

The oscillator strength  $f$  is a number between zero and one that can be thought of as the probability of absorption or emission and hence as the probability that a transition will occur with a photon of a certain energy.

A molecule will absorb light at certain energies depending on which state it is in. The ground-state will absorb different energy photons than an excited state. This fact is used in spectroscopy to

<sup>1</sup>The exact details of the  $\Psi$  functions will be explained in Chapter 2. The notation used is the Dirac bracket notation that allows for convenient integral representations,  $\langle \Psi_f | \hat{\mathbf{r}} | \Psi_i \rangle = \int \Psi_f^*(x_1, x_2, \dots) \hat{\mathbf{r}} \Psi_i(x_1, x_2, \dots) dx_1 dx_2 \dots$

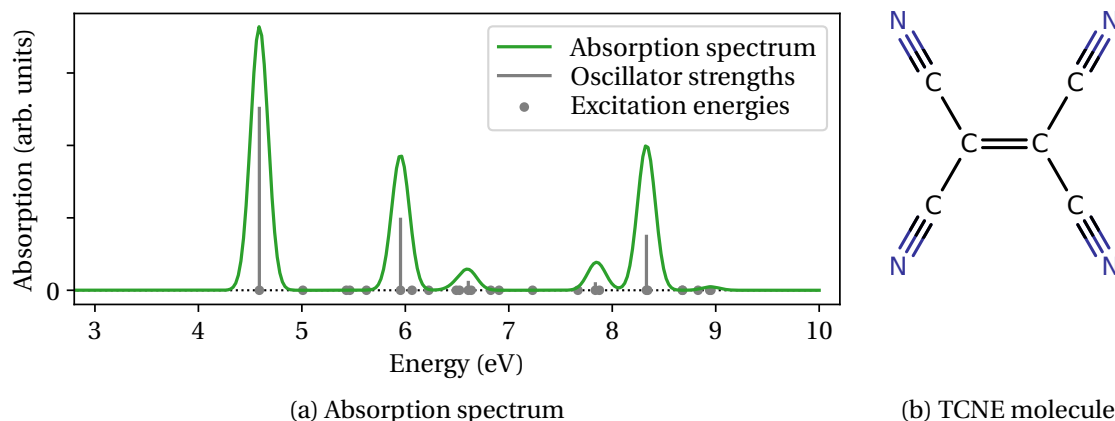


Figure 1.5: An absorption spectrum (a) of TCNE (b) based on a  $GW$ -BSE calculation (this method will be discussed in Section 2.3). Peak locations correspond to the energies of the different neutral excitations of the molecule. The height of the peak corresponds to its oscillator strength. Note that if an excitation has a zero oscillator strength it won't be visible in the spectrum.

identify which states of a molecule are present in a material. As an example we show an absorption spectrum of TCNE in the ground state, see Figure 1.5. Note that the peaks are broadened and not, as one might expect from equation 1.5, sticks. This broadening is due to polarizing effects of the environment and electron-vibration coupling.

### 1.1.3 Processes in Organic Electronics

We have just presented two processes in organic electronics, charge hopping and excitations via photo absorption, here we present a list of all processes that are relevant for organic electronics, and hence, this thesis.

- **Charge transfer:** This is the hopping of electrons and holes from site to site as presented in section 1.1.1.
- **Recombination of electrons and holes:** When a hole and electron meet on the same molecule they can form an exciton or they annihilate one another. In this thesis we assume that annihilation occurs only indirectly via exciton decay.
- **Exciton generation:** If light of the right energy is absorbed an exciton can form.
- **Exciton dissociation:** Excitons can dissociate into a separate electron and hole. This is assumed to be mediated by a charge transfer (CT) state, a state in which the hole and electron are still bound, but are located on neighbouring molecules and no longer on the same molecule.
- **Exciton decay:** An exciton has a finite lifetime after which it falls back to the ground state via photon emission or other path ways.
- **Exciton transfer:** Just like charge carriers also excitons can hop around between sites.

## 1.2 Transient Absorption Spectroscopy

In transient absorption spectroscopy (TAS) not only the species of particles are investigated, but also their time evolution. The main idea of transient absorption spectroscopy is exciting a material with a laser pulse, the pump pulse. Depending on the type of experiment 0.1% to tens of percents of

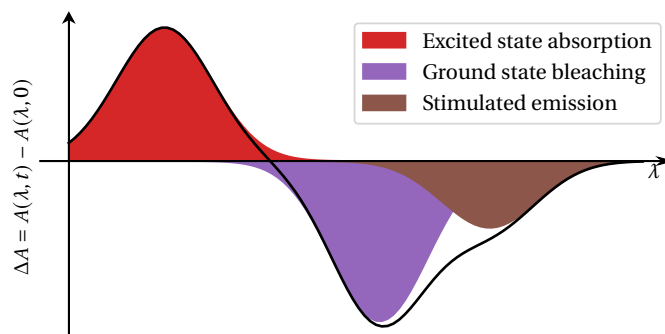


Figure 1.6: An artificial but typical transient absorption spectrum, the black line is  $\Delta A$ , with the three main processes: excited state absorption, groundstate bleaching and stimulated emission.

the molecules get excited [7]. After the system has evolved for a small time interval  $\tau$  (times of 5fs are already possible [8]), the system is probed with a weak laser (such that multiphoton processes are avoided), the probe pulse. The absorption spectrum is recorded for a probe pulse with and without the pump pulse, the difference between the two ( $\Delta A$ ) gives us some indication of what has happened in the time interval. By varying the time interval and the wavelength of light  $\lambda$ , a  $\Delta A(\lambda, \tau)$  profile can be built from which information about the system can be obtained.

In Figure 1.6 we present a typical transient absorption spectrum for a fixed  $\tau$ . Such a spectrum contains information on different processes namely [7]:

1. **Ground-state bleach:** The pump pulse has excited a fraction of the molecules to an excited state, therefore there are less molecules present in the ground state. The probe pulse will thus have a lower absorption in the region of the ground-state.
2. **Stimulated emission:** Already excited states can fall back to the ground-state due to the probe pulse. When this happens the excited state emits a photon. This emitted photon will also result in a perceived lower absorption at the energy of the excited state. This is a process we do not consider in this thesis.
3. **Excited-state absorption:** States excited by the pump pulse can be further excited to higher energies by the probe pulse. This leads to a higher absorption in the transient absorption spectrum.
4. **Other:** Once the material is excited reactions may occur or the exciton may dissociate into a charge transfer state or free charges. This leads to new species in the material that have their own absorption spectrum. This additional absorption may also be visible in the transient absorption spectra.

### 1.3 Multiscale Modelling Approach

In the preceding sections we have seen that the processes involved in organic electronics occur at different scales. There are molecules with their own electronic structure, that combine to form a material. In this material the electronic structure of the molecules changes due to interactions between the molecules that depend on the system morphology. The charge and energy transport processes we are interested in, occur within the electronic structure of the material. To finally arrive at the TAS signal we need to recombine the results of the charge transport model with the absorption spectra of the individual molecules. To develop a model that can assist in the interpretation of TAS signals the multiscale nature of the problem should be taken into account, see Figure 1.7.

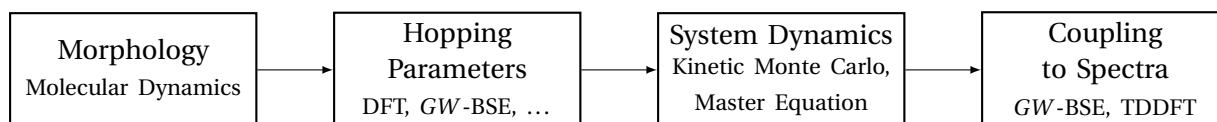


Figure 1.7: The different steps in the multiscale modelling chain needed to arrive at a full model for transient absorption spectra.

First of all the morphology (the positions and orientations of the molecules) of the material needs to be modelled. This can be achieved via Molecular Dynamics (MD), a technique used to model large systems of molecules. A next step is to compute all the site energies and hopping rates needed for the charge and energy transport model. These parameters can be obtained from Density Functional Theory (DFT), more advanced techniques such as *GW*-BSE and multiple other methods that will be discussed in Chapters 2 and 3.

Once the site parameters and rates are known the charge and energy dynamics of the material can be simulated. There are two main approaches to model the dynamics, the Master Equation (ME) and kinetic Monte Carlo (KMC) approach. In the ME approach a balance equation is solved that provides the probability of occupation for every site. From these probabilities properties of the material can be derived such as average absorption spectra, electron mobilities etc. In the KMC approach, the different events are simulated explicitly. In principle both methods give the same results, but both have their own uses and limitations. The ME approach is really inexpensive, large systems can be modelled and results can be obtained within minutes by numerically solving the ME. The main drawback, however, is that only a few (in most cases only one) organic processes can be taken into account at the same time. For example at the moment it is impossible to account for the dissociation of a singlet into a CT state and finally into free charges within the ME approach. The KMC approach is able to account for any process one can think of, but at the cost of a more expensive simulation. In particular simulations for large systems can take days to perform [9]. We discuss the two approaches to charge and energy transport modelling in more detail in Chapter 3.

In the last step the results of the system dynamics should be coupled to the TAS signal. The TAS signal depends on the absorption spectra of the individual molecules. These can be calculated via *GW*-BSE and Time Dependent DFT (TDDFT), two techniques that we discuss in the last two sections of Chapter 2.

## 1.4 Scope and Layout of the Thesis

The central question in this thesis is as follows:

*Is it possible to develop a model that can assist in inferring dynamical processes from transient absorption spectra?*

To answer this question we will first answer the question whether it is possible to numerically model the TAS signal. The methods presented in Chapter 2 and 3 will provide us with an affirmative answer. The next logical question is whether or not the simulated TAS signal gives insight into the processes underlying the signal. To answer this question we apply the multiscale model to a toy system of benzene and TCNE in Chapter 4. In Chapter 5 we summarize the main conclusions and discuss possible future work.

# Chapter 2

## Many-Body Theory of Molecular Systems

In this chapter we introduce the main ideas of the many-body theory of molecular systems. This theory is used to compute geometries and the electronic structure, including spectra, of molecules. We will firstly introduce the part of many-body theory that is relevant for molecules, the theory of many-electron systems, one of the most important approximations in the theory and one of the first approaches to solving the many-electron problem. Thereafter we will discuss three important, more modern, approaches for solving parts of the problem. The first is Density Functional Theory (DFT) a method that is good in predicting ground state properties of materials. The second is known as *GW*-BSE which deals well with excited states and the third method is time-dependent DFT (TDDFT), which is also used for excited state calculations.

### 2.1 Many-Electron Systems

From a chemistry perspective all materials are surprisingly similar on the nanoscale, they consist of only two different types of particles (bodies), the atomic nuclei  $l$  of mass  $M_l$ , charge  $Z_l$  and at position  $\mathbf{R}_l$  and electrons  $i$  with mass  $m$ , charge  $-e$ , spin  $\sigma_i$  and position  $\mathbf{r}_i$ . Furthermore there is predominantly only one interaction between the particles namely the electrostatic or Coulomb interaction. The potential corresponding to this interaction for a particle with unit charge at the origin is

$$v(\mathbf{r}) = \frac{1}{\|\mathbf{r}\|}, \quad (2.1)$$

where we assumed atomic units, i.e.  $m_e = e = \hbar = 4\pi\epsilon_0 = 1$ . The state of the system is described by a wavefunction  $\Psi(\mathbf{x}, t)$ , where  $\mathbf{x}$  contains all time-independent variables (i.e.  $\mathbf{x} = \{\{\mathbf{r}_i, \sigma_i\}, \{Z_l, \mathbf{R}_l\}\}$ ) and  $t$  represents time. The dynamics of the system are governed by the system's Hamiltonian  $\hat{H}_{\text{sys}}$  via the Schrödinger equation

$$i \frac{\partial \Psi}{\partial t} = \hat{H}_{\text{sys}} \Psi, \quad (2.2)$$

with  $\hat{H}_{\text{sys}}$  given by

$$\begin{aligned} \hat{H}_{\text{sys}} = & \frac{1}{2} \sum_l \frac{1}{M_l} \mathbf{P}_l^2 + \frac{1}{2} \sum_i \mathbf{p}_i^2 + \frac{1}{2} \sum_{\substack{l,l' \\ (l \neq l')}} Z_l Z_{l'} v(\mathbf{R}_l - \mathbf{R}_{l'}) \\ & - \sum_l \sum_i Z_l v(\mathbf{r}_i - \mathbf{R}_l) + \frac{1}{2} \sum_{\substack{i,i' \\ (i \neq i')}} v(\mathbf{r}_i - \mathbf{r}_{i'}), \end{aligned} \quad (2.3)$$

where we introduced the momentum operators  $\mathbf{P}_l = -i\nabla_{\mathbf{R}_l}$  and  $\mathbf{p}_i = -i\nabla_{\mathbf{r}_i}$ . In equation (2.3) we have from left to right, the kinetic energy of the nuclei, the kinetic energy of the electrons, the nucleus-nucleus interactions, the nucleus-electron interactions and finally the electron-electron

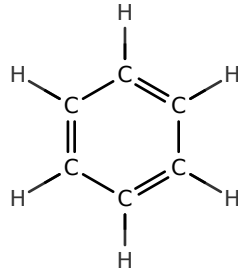


Figure 2.1: A benzene molecule.

interactions. Note that the Hamiltonian (2.3) does not depend on time. We therefore split the wavefunction in a product of spatial and temporal terms, i.e.  $\Psi(\mathbf{x}, t) = \Psi(\mathbf{x})f(t)$ . This allows us to apply separation of variables

$$i \frac{1}{f(t)} \frac{\partial f}{\partial t} = \frac{1}{\Psi(\mathbf{x})} \hat{H}_{\text{sys}} \Psi(\mathbf{x}), \quad (2.4)$$

and since the left side only depends on  $t$  and the right only on  $\mathbf{x}$ , both sides must be equal to a constant. This constant is the energy  $E$  of the system, solving both parts separately gives the time-independent Schrödinger equation

$$\hat{H}_{\text{sys}} \Psi(\{\mathbf{r}_i, \sigma_i\}, \{Z_l, \mathbf{R}_l\}) = E \Psi(\{\mathbf{r}_i, \sigma_i\}, \{Z_l, \mathbf{R}_l\}) \quad (2.5)$$

and the time evolution of the system

$$f(t) = e^{-iEt}. \quad (2.6)$$

Since the Hamiltonian does not depend on the spin of the electrons, we will ignore the spin of the electrons for now and reintroduce it when it is necessary (i.e.  $\Psi = \Psi(\{\mathbf{r}_i\}, \{Z_l, \mathbf{R}_l\})$ ).

In principle all properties (geometric structure, spectra etc.) of the system can be computed from equation (2.5). In practice however we run into problems quickly. Due to all the interacting terms, equation (2.5) forms a system of coupled differential equations that cannot be split into smaller systems and the number of variables in the system is large. For example, a single benzene molecule, see Figure 2.1, with 12 nuclei and 42 electrons already leads to a problem of 162 spatial variables. Therefore solving equation (2.5) for any reasonable molecule is impossible no matter what numerical methods are used.

### 2.1.1 The Born-Oppenheimer Approximation

To be able to do anything with equation (2.5) we need approximations. The first approximation we make is the Born-Oppenheimer approximation [10]. An obvious observation is that nuclei are more massive than electrons at least by a factor of 1836. Therefore the dynamics of nuclei will be much slower than the dynamics of the electrons. Electrons will follow the movement of the nuclei almost instantaneously while the nuclei are not able to follow the motions of the electrons, but only experience a time averaged potential.

In the Born-Oppenheimer approximation we decouple the motions of the electrons from the motions of the nuclei. We treat the nuclei as fixed in space which lead to a reformulation of the wavefunction

$$\Psi(\{\mathbf{r}_i\}, \{Z_l, \mathbf{R}_l\}) = \Psi_e(\{\mathbf{r}_i\}; \{Z_l, \mathbf{R}_l\}) \cdot \Psi_n(\{Z_l, \mathbf{R}_l\}) \quad (2.7)$$

and the electronic Schrödinger equation

$$\hat{H}_e \Psi_e(\{\mathbf{r}_i\}; \{Z_l, \mathbf{R}_l\}) = E \Psi_e(\{\mathbf{r}_i\}; \{Z_l, \mathbf{R}_l\}). \quad (2.8)$$

Since we assume the nuclei are fixed the nuclear part of the wavefunction cancels out in the Schrödinger equation and the positions and charges of the nuclei only enter in the equation as parameters, no longer as variables (denoted by the semicolon). The Hamiltonian is also simpler now: we can ignore the kinetic energy of the nuclei and treat the electron-nuclei interaction as the interaction of the electrons with a fixed (external) potential i.e.

$$V_n(\mathbf{r}) = - \sum_l Z_l v(\mathbf{r} - \mathbf{R}_l), \quad (2.9)$$

for an electron at position  $\mathbf{r}$ . Furthermore the nucleus-nucleus interaction in the Hamiltonian is now a constant and hence will only lead to an energy shift by a fixed value. The Hamiltonian  $\hat{H}_e$  is therefore given by

$$\hat{H}_e = \frac{1}{2} \sum_i \mathbf{p}_i^2 + \sum_i V_n(\mathbf{r}_i) + \frac{1}{2} \sum_{\substack{i,i' \\ (i \neq i')}} v(\mathbf{r}_i - \mathbf{r}_{i'}) \quad (2.10)$$

where we have from left to right the kinetic energy of the electrons, the interaction with the potential energy from the field of nuclei and the electron-electron interaction.

Above we have presented the Born-Oppenheimer approximation from a classical point of view. The original approximation was obtained by studying a perturbation of the time-independent Hamiltonian, with respect to the mass ratio of the electron and proton. It was shown that the interaction with the nuclei does not lead to transitions of the electrons between stationary states. This is called the adiabatic approximation. This is the actual justification of the decoupling of the movements of the nuclei and electrons, more details can be found in the first chapters of [11] and [12].

### 2.1.2 The Wavefunction and the Variational Principle

With the Born-Oppenheimer approximation we have reduced the many-body problem to a many-electron problem, that obeys the following electronic Schrödinger equation

$$\hat{H}_e \Psi = E \Psi, \quad (2.11)$$

where we dropped the subscript  $e$  of the wavefunction. To solve this equation we need to know more about the wavefunction and its interpretation in a physical and chemical context. The wavefunction  $\Psi$  describes the state of the whole  $N$ -electron system, in particular  $|\Psi|^2$  can be interpreted as a probability distribution.  $|\Psi(\mathbf{r}_1, \dots, \mathbf{r}_N)|^2$  is the probability of finding the system in a state where particle  $i$  is at location  $\mathbf{r}_i$ . From this we derive a first condition on the wavefunction

$$\int |\Psi(\mathbf{r}_1, \dots, \mathbf{r}_N)|^2 d\mathbf{r}^N = 1 \quad (2.12)$$

where  $d\mathbf{r}^N = d\mathbf{r}_1 \dots d\mathbf{r}_N$ . The wavefunction must also be antisymmetric with respect to particle exchange

$$\Psi(\mathbf{r}_1, \dots, \mathbf{r}_k, \mathbf{r}_l, \dots, \mathbf{r}_N) = -\Psi(\mathbf{r}_1, \dots, \mathbf{r}_l, \mathbf{r}_k, \dots, \mathbf{r}_N). \quad (2.13)$$

This condition stems from the Pauli exclusion principle that states that no two fermions (electrons are fermions) can be in the same state at the same time.

Solving equation (2.11) for  $E$  and  $\Psi$  is an eigenvalue problem and solutions are given by eigenvalues  $E_k$  and corresponding eigenfunctions  $\Psi_k$ . The set of eigenfunctions is complete and can always be taken orthogonal and normalized

$$\int \Psi_k^* \Psi_l d\mathbf{r}^N = \langle \Psi_k^* | \Psi_l \rangle = \delta_{kl}. \quad (2.14)$$

The values  $E_k$  are the energies of the system, we will assume throughout the rest of this thesis that the energies are ordered  $E_0 \leq E_1 \leq \dots$ . We call the lowest energy  $E_0$  of the system the ground-state. The higher states are called excited states and  $E_k$  is the energy of the  $k$ th excited state.

To extract information from the wavefunction we can apply operators to it. Every observable (measurable quantity) has its own operator, like the Hamiltonian for the energy. For a general observable with operator  $\hat{A}$  we can find the expectation value of that observable via

$$\langle \hat{A} \rangle = \frac{\int \Psi^* \hat{A} \Psi \, d\mathbf{r}^N}{\int \Psi^* \Psi \, d\mathbf{r}^N} = \frac{\langle \Psi | \hat{A} | \Psi \rangle}{\langle \Psi | \Psi \rangle}. \quad (2.15)$$

Note that if  $\Psi$  is normalized the expression simplifies to  $\langle \hat{A} \rangle = \langle \Psi | \hat{A} | \Psi \rangle$ . Furthermore the expectation value of an observable gives us a number as a function of  $\Psi$  and hence we can see the expectation value of an observable as a functional of  $\Psi$  i.e.  $\langle \hat{A} \rangle = A[\Psi]$ .

### The Variational Principle

A very important quantity of a many-electron system is its ground-state. To find the ground-state we can use a variational principle. It states that for every trial wavefunction  $\Psi_{\text{trial}}$  we have for the energy  $E$

$$E[\Psi_{\text{trial}}] \geq E_0. \quad (2.16)$$

This implies that the ground-state energy is given by

$$E_0 = \min_{\Psi} E[\Psi]. \quad (2.17)$$

Note that this gives us an alternative way of solving the original Schrödinger equation for the ground-state, namely by minimizing the functional  $E$ . We can prove this result if we consider the normalized and orthogonal eigenfunctions  $\psi_k$  of the energy operator  $\hat{H}_e$  with ordered eigenvalues  $E_0 \leq E_1 \leq \dots$ . Since the eigenfunctions form a complete basis we can expand any normalized state  $|\Psi\rangle$  as

$$|\Psi\rangle = \sum_n c_n |\psi_n\rangle. \quad (2.18)$$

Therefore we have

$$\begin{aligned} \langle \Psi | \hat{H}_e | \Psi \rangle &= \left( \sum_n c_n^* \langle \psi_n | \right) \hat{H}_e \left( \sum_n c_n |\psi_n\rangle \right) \\ &= \sum_{m,n} c_m^* c_n \langle \psi_m | \hat{H}_e | \psi_n \rangle \\ &= \sum_{m,n} c_m^* c_n \langle \psi_m | E_n | \psi_n \rangle \\ &= \sum_{m,n} c_m^* c_n E_n \langle \psi_m | \psi_n \rangle \\ &= \sum_n |c_n|^2 E_n \\ &\geq \sum_n |c_n|^2 E_0 = E_0. \end{aligned} \quad (2.19)$$

where we used in the last line that for a normalized state  $\sum_n |c_n|^2 = 1$ .

To make the minimization “computer solvable” we can reformulate it as a constrained minimization in terms of Lagrange multipliers with the constraint  $\langle \Psi | \Psi \rangle = 1$

$$\delta [\langle \Psi | \hat{H}_e | \Psi \rangle - E \langle \Psi | \Psi \rangle] = 0, \quad (2.20)$$

where  $E$  takes the role of the Lagrange multiplier.

### 2.1.3 Non-interacting Electrons

To use the variational principle we need a trial wavefunction. To find a trial wavefunction we will first look at a special limiting case in which the electrons of the system do not interact. The Hamiltonian of such a system is

$$\hat{H} = \sum_{i=1}^N \hat{h}_i \quad (2.21)$$

with the single-particle Hamiltonian given by

$$\hat{h}_i = \frac{1}{2} \hat{\mathbf{p}}_i^2 - V_n(\mathbf{x}_i). \quad (2.22)$$

Here  $\mathbf{x}_i$  is a variable containing both the position and spin of electron  $i$  or if we neglect spin only the position. The single particle Hamiltonian has a corresponding set of eigenfunctions  $\psi_k$  (also called spin orbitals) and eigenvalues  $\varepsilon_k$

$$\hat{h}_i \psi_k = \varepsilon_k \psi_k. \quad (2.23)$$

Since the particles do not interact they are independent and their total wavefunction can be written as a product of the single particle wavefunctions, the Hartree product

$$\Psi(\mathbf{x}_1, \mathbf{x}_2, \dots) = \psi_i(\mathbf{x}_1) \psi_k(\mathbf{x}_2) \dots \quad (2.24)$$

It is easily shown that indeed  $\Psi$  is an eigenfunction of  $\hat{H}$ , take for example a non-interacting two electron system, i.e.  $\hat{H} = \hat{h}_1 + \hat{h}_2$  then

$$\hat{H}\Psi = (\hat{h}_1 + \hat{h}_2) \psi_i(\mathbf{x}_1) \psi_k(\mathbf{x}_2) \quad (2.25)$$

$$= \hat{h}_1 \psi_i(\mathbf{x}_1) \psi_k(\mathbf{x}_2) + \hat{h}_2 \psi_i(\mathbf{x}_1) \psi_k(\mathbf{x}_2) \quad (2.26)$$

$$= \varepsilon_i \psi_i(\mathbf{x}_1) \psi_k(\mathbf{x}_2) + \psi_i(\mathbf{x}_1) \varepsilon_k \psi_k(\mathbf{x}_2) \quad (2.27)$$

$$= (\varepsilon_i + \varepsilon_k) \psi_i(\mathbf{x}_1) \psi_k(\mathbf{x}_2) \quad (2.28)$$

$$= (\varepsilon_i + \varepsilon_k) \Psi. \quad (2.29)$$

From this we deduce that the Hartree product is a solution to the non-interacting many electron problem and furthermore that the energy of the system is equal to the sum of the electron energies. The Hartree product is unphysical, it uses the fact that we can label the electrons as electron 1, electron 2 etc. Electrons are however indistinguishable and the wavefunction must be anti-symmetric with respect to electron exchange, see Equation (2.13). This is provided by the Hartree-Fock approximation.

### 2.1.4 The Hartree-Fock Approximation

The Hartree-Fock approximation makes use of an anti-symmetrized version of the Hartree product. The antisymmetrization is achieved by taking a determinant of the single particle wavefunctions, the so-called Slater determinant,

$$\Psi^{\text{HF}} = \frac{1}{\sqrt{N!}} \begin{vmatrix} \psi_1(\mathbf{x}_1) & \psi_1(\mathbf{x}_2) & \cdots & \psi_1(\mathbf{x}_N) \\ \psi_2(\mathbf{x}_1) & \psi_2(\mathbf{x}_2) & \cdots & \psi_2(\mathbf{x}_N) \\ \vdots & \vdots & \ddots & \vdots \\ \psi_N(\mathbf{x}_1) & \psi_N(\mathbf{x}_2) & \cdots & \psi_N(\mathbf{x}_N) \end{vmatrix} \quad (2.30)$$

$$= |\psi_1(\mathbf{x}_1) \psi_2(\mathbf{x}_2) \cdots \psi_N(\mathbf{x}_N)|. \quad (2.31)$$

Here  $\mathbf{x}_i$  is a variable containing both the position and spin of electron  $i$ . If we however neglect spin every single particle wavefunction can contain two electrons and hence the  $\psi_i$ s in the Slater determinant do not go to  $N$  but  $N/2$ .

The expectation value (in atomic units) of the energy for  $\Psi^{\text{HF}}$  is

$$E_{\text{HF}} = \langle \Psi^{\text{HF}} | \hat{H} | \Psi^{\text{HF}} \rangle = \sum_i H_i + \frac{1}{2} \sum_{i,j} (J_{ij} - K_{ij}) \quad (2.32)$$

$$H_i = \int \psi_i^*(\mathbf{x}) \left[ -\frac{1}{2} \nabla^2 - v(\mathbf{x}) \right] \psi_i(\mathbf{x}) d\mathbf{x} \quad (2.33)$$

$$J_{ij} = \iint \psi_i(\mathbf{x}_1) \psi_i^*(\mathbf{x}_1) \frac{1}{r_{12}} \psi_j^*(\mathbf{x}_2) \psi_j(\mathbf{x}_2) d\mathbf{x}_1 d\mathbf{x}_2 \quad (2.34)$$

$$K_{ij} = \iint \psi_j^*(\mathbf{x}_1) \psi_i(\mathbf{x}_1) \frac{1}{r_{12}} \psi_i(\mathbf{x}_2) \psi_j^*(\mathbf{x}_2) d\mathbf{x}_1 d\mathbf{x}_2. \quad (2.35)$$

$H_i$  is the single particle energy due to the kinetic energy and its interaction with the potential of the nuclei.  $J_{ij}$  is called the Coulomb integral, and is exactly that, it contains an average Coulomb interaction between the electrons. The final term  $K_{ij}$  is called the exchange integral and results from the antisymmetry property. Note that  $K_{ii} = J_{ii}$  and therefore the sum can be taken over all pairs since the self interaction of the electron cancels, to compensate for double counting a factor half is added to the interaction terms.

Now that we have a trial wave function and a way to compute its energy we can apply the variational principle. From which we obtain the Hartree-Fock equations

$$\hat{h}_i \psi_i = \epsilon_i \psi_i, \quad i = 1, \dots, N \quad (2.36)$$

where  $\hat{h}$  is a single particle operator, called the Fock operator. The Lagrange multipliers  $\epsilon_i$  can be identified as orbital energies for orbital  $\psi_i$  according to Koopmans theorem [13], which states that the energy associated with removing an electron from  $\psi_i$  is approximately equal to  $-\epsilon_i$ .  $\hat{h}$  is given by

$$\hat{h}_i = -\frac{1}{2} \nabla_i^2 + V_n(\mathbf{x}_i) + V_{\text{HF}}(\mathbf{x}_i) \quad (2.37)$$

where the first two terms are again the kinetic energy and potential due to the nuclei and  $V_{\text{HF}}$  is the Hartree-Fock potential given by

$$V_{\text{HF}}(\mathbf{x}_i) = \sum_j (J_j(\mathbf{x}_i) - K_j(\mathbf{x}_i)) \quad (2.38)$$

$$J_j(\mathbf{x}_i) = \int |\psi_j(\mathbf{x}_2)|^2 \frac{1}{r_{i2}} d\mathbf{x}_2 \quad (2.39)$$

$$K_j(\mathbf{x}_i) \psi_i(\mathbf{x}_i) = \int \psi_j^*(\mathbf{x}_2) \frac{1}{r_{i2}} \psi_i(\mathbf{x}_2) d\mathbf{x}_2 \psi_j(\mathbf{x}_i). \quad (2.40)$$

$J_j$  is the average Coulomb potential experienced by an electron due to another electron in orbital  $j$  and  $K_j$  is again a term due to the antisymmetry. It is called the exchange term, but unfortunately no intuitive (classical) explanation exists for it.

### 2.1.5 Solving the Hartree-Fock equation

From the variational principle and the Hartree-Fock approximation we have obtained a set of equations (2.36) that once solved give an approximation for the ground state. But an important question is unanswered, how to solve equations (2.36)? To solve the equations we need to vary the functions

$\psi_i$ . For a computer this is very hard and almost impossible, a way around this is to expand each  $\psi_i$  in some basis of functions i.e.

$$\psi_i = \sum_j^M c_{ij} \phi_j. \quad (2.41)$$

where the  $\phi_j$  are known functions and  $M$  is the size of the basis set. By varying the coefficients  $c_{ij}$  we can vary  $\psi_i$ . This is exactly what is done in computational chemistry. Substitution of (2.41) in (2.36) and multiplying from the left with  $\phi_l$  gives

$$\sum_j^M c_{ij} \langle \phi_l | \hat{h}_i | \phi_j \rangle = \sum_j^M \epsilon_i c_{ij} \langle \phi_l | \phi_j \rangle, \quad (2.42)$$

which can be expressed in a matrix form

$$\mathbf{F}\mathbf{C}_i = \epsilon_i \mathbf{S}\mathbf{C}_i \quad (2.43)$$

where  $\mathbf{F}$  is the Fock matrix with  $F_{lj} = \langle \phi_l | \hat{h}_i | \phi_j \rangle$ ,  $\mathbf{S}$  is the overlap matrix with  $S_{lj} = \langle \phi_l | \phi_j \rangle$  and  $\mathbf{C}_i$  is a vector containing all coefficients  $c_{ij}$  for fixed  $i$ . This equation is known as the Roothaan equation [14] who derived it in 1951.

The Roothaan equations can be solved with the help of linear algebra techniques on a computer. It is however important to realize that  $\mathbf{F}$  depends on the values of the orbitals  $\psi_i$  via the Hamiltonian. Therefore, we need a special approach to solve equations (2.43). We start with a guess for the orbitals, compute the Hamiltonian and  $\mathbf{F}$  based on this guess, and then solve the linear system. The solution is used as a new guess to recompute the Hamiltonian and  $\mathbf{F}$  and then the system is solved again. This is repeated until the input matches the output. This approach is called the Self Consistent Field (SCF) approach.

### 2.1.6 Basis sets

The choice of basis set is very important, since we expand  $\psi_j$  in terms of basis functions the accuracy of the solution comes, in a large part, down to how well the basis functions can describe the true wavefunctions  $\psi_i$ .

To make sure that the  $\psi_i$  can be approximated rather well,  $\phi_i$ s are generally approximations to the true atomic orbitals of an atom. These atomic orbitals can however be nasty to work with, therefore they are once again expanded in a basis and most frequently [15] in a basis of Gaussian-type functions

$$\phi_i = \sum_{\mu} a_{\mu i} \chi_{\mu} \quad (2.44)$$

where  $\chi_{\mu}$  are Gaussian functions. Gaussian functions are so popular because their product can be easily (and analytically) evaluated, this results in easy evaluation of two-electron integrals. These basis functions are called contracted Gaussian-type basis functions.

For contracted Gaussian-type basis functions a large number of basis sets exist. There exist so many basis sets because in general larger basis sets will give better results, but will also lead to higher computational cost. Furthermore for some calculations particular extra functions are needed that can be omitted in other calculations. Hence the selection of the correct basis set is application specific. A brief overview of some of the types of basis sets, for more details see for example [16]:

- **Minimum or Single Zeta:** The minimum basis set is what the name implies it is the smallest possible basis set and has one contracted Gaussian for every atomic orbital (e.g. for elements in the second row of the periodic system we have two s-functions and one set of p functions,  $p_x$ ,  $p_y$  and  $p_z$ ).

- **Double, Triple, ... Zeta:** The minimum basis sets are usually improved by adding more functions per atomic orbital. A double zeta (DZ) basis has double the number of functions per atomic orbital, a triple zeta (TZ) basis triple the number of functions etc. The benefit from more functions is that it allows for more freedom in the distributions of the electrons around the atoms. This is particularly useful for molecules in which different electrons of the same orbital are in different bond types. There are also split valence basis sets in these sets not all orbitals are doubled or tripled but only the valence orbitals.
- **Polarization functions:** To allow for the polarization of a molecule, higher angular momentum functions are essential. They provide the electrons with the freedom to form asymmetric distributions around the nucleus. In general just the first empty higher angular momentum function is added, i.e. for a p orbital an extra d orbital will be added and for a d orbital an f orbital.
- **Diffuse functions:** Diffuse functions can also be added. These are functions with a small exponent of the Gaussian such that they have a long tail and hence are good at describing electrons that are delocalized. This is important for charged molecules and dipole moments.

### 2.1.7 Limitations of the Hartree-Fock Approach

The Hartree-Fock approach gives us a first approximation to the groundstate. The approach however has some limitations and drawbacks.

- The Hartree-Fock potential  $V_{\text{HF}}$  is non-local and depends on the spin orbitals. Therefore the SCF approach is needed.
- Since the Hartree-Fock approximation only uses a single Slater determinant correlation effects of the electrons cannot be taken into account. Correlation is the fact that electrons repel, hence around every electron you expect an exclusion zone where no other electrons are found. This exclusion is however not taken into account and interactions with other electrons are included only as an averaged effect (mean field).

It seems that in particular the last point could be solved by taking a combination of Slater determinants as the approximate wavefunction. This is done for example in the Configuration Interaction approach [17] and the Coupled-Cluster approach [18]. We however will pursue a different approach that is centered around the electron density.

## 2.2 Density Functional Theory

In the previous section we presented a wavefunction oriented approach to solving the  $N$ -electron problem (2.11). The wavefunction depends on at least  $3N$  spatial variables for the electrons. In 1964 a paper was published by Hohenberg and Kohn in which they showed that the electron density,

$$n(\mathbf{r}_1) = N \int |\Psi(\mathbf{r}_1, \mathbf{r}_2, \dots, \mathbf{r}_N)|^2 d\mathbf{r}_2 \dots d\mathbf{r}_N, \quad (2.45)$$

determines the ground state uniquely up to an “uninteresting additive constant” [19]. Every observable in the ground state can thus be computed from the density. This implies that we can reduce the problem complexity and go from a problem with  $3N$  variables to a problem with just 3. This is the basic idea behind Density Functional Theory (DFT) for which Walter Kohn received the Nobel prize in 1998.

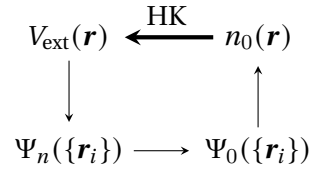


Figure 2.2: A visual representation of the result given by the first Hohenberg-Kohn theorem, indicated by the thick arrow labelled HK.

We start by discussing the two main theorems showing that indeed the electron density can be used to uniquely find the ground state and give a way of computing the ground state energy. Thereafter we present a way of using the electron density to compute the ground state via the Kohn-Sham equations and finally we discuss the different functionals used in DFT.

### 2.2.1 The Hohenberg-Kohn Theorems

We consider again the  $N$ -electron problem

$$\left[ \sum_i -\frac{1}{2} \nabla^2 + \sum_i V_{\text{ext}}(\mathbf{r}_i) + \frac{1}{2} \sum_{\substack{i,i' \\ (i \neq i')}} v(\mathbf{r}_i - \mathbf{r}_{i'}) \right] \Psi = E\Psi, \quad (2.46)$$

$$[\hat{T} + \hat{V} + \hat{U}] \Psi = E\Psi, \quad (2.47)$$

where the first term is the kinetic energy, the second term the external potential (containing the potential from the nuclei and any other external potential) and the last term the Coulomb interaction. For simplicity we will assume that the ground state is non-degenerate.

Note that in equation (2.46) the solution  $\Psi$  depends only on the external potential  $V_{\text{ext}}$  and the number of electrons  $N$ . The rest of the Hamiltonian is equal for any  $N$ -electron system. Furthermore since the ground state is unique, the ground state density is uniquely determined by  $V_{\text{ext}}$  and  $N$ . The first Hohenberg-Kohn theorem shows the reverse namely that the ground state density  $n_0(\mathbf{r})$  determines the external potential  $V_{\text{ext}}$  uniquely up to a constant.

To see the use of this result, consider Figure 2.2. Via the thin arrows we can go from the potential  $V_{\text{ext}}$  to the wavefunction, to the ground state and finally to the ground state electron density, this is what we do when we solve the Schrödinger equation. With the Hohenberg-Kohn theorem we will also be able to go from the ground state density to the potential (thick arrow) and to the wavefunction. Hence it allows us to use the electron density as the basic variable in our computations.

**Theorem 1** (Hohenberg-Kohn I). *For any electronic system in an external potential  $V_{\text{ext}}$  the potential is uniquely determined, up to a constant, by the ground state density  $n_0(\mathbf{r})$ .*

The proof of this theorem is relatively easy and is given by a reduction ad absurdum [20].

*Proof.* Suppose there is another potential  $V'(\mathbf{r})$  with ground state  $\Psi'$  that gives rise to the same ground state density  $n_0(\mathbf{r})$ . Then  $\Psi'$  cannot be equal to  $\Psi$ , unless they differ by a constant, since they satisfy different Schrödinger equations. Let  $E, E'$  and  $H, H'$  denote the energy and Hamiltonian of the non-primed and primed ground state then we have by the variational principle

$$E = \langle \Psi | H | \Psi \rangle < \langle \Psi' | H | \Psi' \rangle = \langle \Psi' | H + V_{\text{ext}} - V' | \Psi' \rangle \quad (2.48)$$

$$\implies E < E' + \int (V_{\text{ext}}(\mathbf{r}) - V'(\mathbf{r})) n_0(\mathbf{r}) d\mathbf{r}, \quad (2.49)$$

but we also have

$$E' = \langle \Psi' | H' | \Psi' \rangle < \langle \Psi | H' | \Psi \rangle = \langle \Psi | H' + V' - V_{\text{ext}} | \Psi \rangle \quad (2.50)$$

$$\implies E' < E + \int (V'(\mathbf{r}) - V_{\text{ext}}(\mathbf{r})) n_0(\mathbf{r}) d\mathbf{r}, \quad (2.51)$$

which finally leads to a contradiction

$$E + E' < E + E'. \quad (2.52)$$

□

Thus both potentials need to be the same (at least up to a constant). This implies that the potential  $V_{\text{ext}}$  is uniquely determined by (i.e. a functional of) the density and since the potential defines the Hamiltonian, also the ground state wavefunction is a functional of the electron density, see Figure 2.2. From this it follows that also the kinetic and interaction (Coulomb) energy are a functional of the electron density. Therefore we can define

$$F[n(\mathbf{r})] \equiv \langle \Psi | \hat{T} + \hat{U} | \Psi \rangle, \quad (2.53)$$

where  $F$  is a general functional that accounts for the kinetic and interaction energy. Using  $F$  we can define a functional for the total energy

$$E[n(\mathbf{r})] \equiv F[n(\mathbf{r})] + \int V_{\text{ext}}(\mathbf{r}) n(\mathbf{r}) d\mathbf{r}. \quad (2.54)$$

To compute the ground state energy we need more than just this functional. In the Hartree-Fock approach we got the energy via the variational principle, it would be nice to have a similar principle for (2.54) and that is exactly what the second Hohenberg-Kohn theorem [20] is about.

**Theorem 2** (Hohenberg-Kohn II). *For any trial density  $\tilde{n}(\mathbf{r})$  such that  $\tilde{n}(\mathbf{r}) \geq 0$  and  $\int \tilde{n}(\mathbf{r}) d\mathbf{r} = N$ , we have*

$$E[\tilde{n}(\mathbf{r})] \geq E_0. \quad (2.55)$$

The proof is based around the fact that every trial density has its own unique potential  $\tilde{V}$  and therefore Hamiltonian  $\tilde{H}$  and corresponding wavefunction  $\tilde{\Psi}$ .

*Proof.* Take the wavefunction corresponding to the trial density  $\tilde{n}(\mathbf{r})$ , then we have

$$\langle \tilde{\Psi} | \hat{H} | \tilde{\Psi} \rangle = \langle \tilde{\Psi} | \hat{T} + \hat{U} | \tilde{\Psi} \rangle + \langle \tilde{\Psi} | \tilde{V} | \tilde{\Psi} \rangle \quad (2.56)$$

$$= F[\tilde{n}(\mathbf{r})] + \int V_{\text{ext}}(\mathbf{r}) \tilde{n}(\mathbf{r}) d\mathbf{r}. \quad (2.57)$$

From the variational principle we have  $\langle \tilde{\Psi} | \hat{H} | \tilde{\Psi} \rangle \geq \langle \Psi_0 | \hat{H} | \Psi_0 \rangle = E_0$  where  $\Psi_0$  is the true ground state. Thus we also have

$$F[\tilde{n}(\mathbf{r})] + \int V_{\text{ext}}(\mathbf{r}) \tilde{n}(\mathbf{r}) d\mathbf{r} \geq F[n_0(\mathbf{r})] + \int V_{\text{ext}}(\mathbf{r}) n_0(\mathbf{r}) d\mathbf{r} \quad (2.58)$$

$$= \langle \Psi_0 | \hat{H} | \Psi_0 \rangle = E_0. \quad (2.59)$$

This proves the variational principle for the energy as a functional of the electron density. □

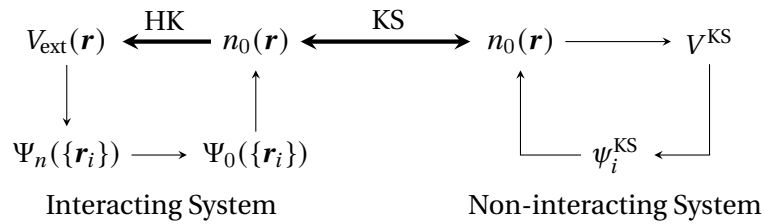


Figure 2.3: A visual representation of the function of the Kohn-Sham idea. The idea is to solve a system of non-interacting particles with the same density as the original problem.

This result seems extraordinary, but some care needs to be taken. In the first Hohenberg-Kohn theorem we use the fact that for a given potential  $V_{\text{ext}}$  there is a  $n_0(\mathbf{r})$  which uniquely determines  $V_{\text{ext}}$ . It is however not necessarily the case that any ground state density  $n_0(\mathbf{r})$  has an associated potential  $V_{\text{ext}}$ . Hence the Hohenberg-Kohn theorems only work for densities that are  $V$ -representable, i.e. which have a potential associated to them. Hohenberg and Kohn however, mention in a footnote in their paper that they *expect* that all except some pathological distributions can be realized by some potential [20]. For a more detailed discussion on this subject see for example section 3.3 of [21].

Given the results of Hohenberg and Kohn we could in principle find the ground state density, using the variational principle. The ground state that we find is in principle exact, we have not made any approximations or put restraints on the shape of the wavefunction (as we did with Hartree-Fock). Nonetheless this Hohenberg-Kohn-DFT is never really used, since it still involves difficult interaction terms. Instead an approach is used that was proposed by Kohn and Sham.

## 2.2.2 The Kohn-Sham Equations

In 1965 Kohn and Sham published a paper [22] in which they proposed a method to use the electron density to solve the  $N$ -electron problem for the ground state. The main idea behind their approach is the assumption that the ground state density of the true system is equal to that of a (easily) solvable non-interacting system, where all the difficult parts (exchange and correlation) are collected in some approximate functional. A visual representation of this idea can be found in Figure 2.3.

To make the connection between a non-interacting and an interacting system Kohn and Sham separated the functional  $F[n(\mathbf{r})]$

$$F[n] = T_s[n] + J[n] + E_{xc}[n] \quad (2.60)$$

$$T_s[n] = -\frac{1}{2} \sum_i \langle \psi_i | \nabla^2 | \psi_i \rangle \quad (2.61)$$

$$J[n] = \frac{1}{2} \iint \frac{n(\mathbf{r})n(\mathbf{r}')}{|\mathbf{r} - \mathbf{r}'|} d\mathbf{r} d\mathbf{r}' \quad (2.62)$$

$$E_{xc}[n] = (T[n] - T_s[n]) + (V_{ee}[n] - J[n]). \quad (2.63)$$

$T_s[n]$  is the kinetic energy of a non-interacting electron system,  $J[n]$  describes an average Coulomb interaction and  $E_{xc}$  (the exchange-correlation functional) is a correction that accounts for the difference between the non-interacting and interacting system.

Remember that for the energy functional  $E[n]$  we have a variational principle, to find the ground-state we should minimize  $E$  as a functional of  $n$ . Reformulating this with the constraint  $\int n(\mathbf{r}) d\mathbf{r} = N$  in terms of Lagrange multipliers gives

$$\frac{\delta}{\delta n(\mathbf{r})} \left[ E[n(\mathbf{r})] - \mu \int n(\mathbf{r}) d\mathbf{r} \right] = 0 \quad (2.64)$$

with  $\mu$  the Lagrange multiplier and the corresponding Euler equation

$$\mu = \frac{\delta E[n(\mathbf{r})]}{\delta n(\mathbf{r})} \quad (2.65)$$

$$= \frac{\delta T_s[n(\mathbf{r})]}{\delta n(\mathbf{r})} + V_{\text{eff}}(\mathbf{r}), \quad (2.66)$$

where we substituted (2.54) for the energy and used the splitting of  $F[n]$  (2.60), furthermore

$$V_{\text{eff}} = V_{\text{ext}}(\mathbf{r}) + \int \frac{n(\mathbf{r}')}{|\mathbf{r} - \mathbf{r}'|} d\mathbf{r}' + V_{\text{xc}}(\mathbf{r}), \quad (2.67)$$

$$V_{\text{xc}}(\mathbf{r}) = \frac{\delta E_{\text{xc}}[n(\mathbf{r})]}{\delta n(\mathbf{r})} \quad (2.68)$$

Equation (2.66) tells us what we need, it states that we can rewrite our original problem as a problem of non-interacting particles with kinetic energy  $T_s[n]$  moving around in effective potential  $V_{\text{eff}}$ . The non-interacting part implies that we can write the wave function in the Slater determinant form and moreover that we can use single particle Schrödinger equations to solve the problem

$$\left[ -\frac{1}{2}\nabla^2 + V_{\text{eff}}(\mathbf{r}) \right] \psi_i^{\text{KS}} = \epsilon_i^{\text{KS}} \psi_i^{\text{KS}}, \quad i = 1, \dots, N \quad (2.69)$$

and

$$n(\mathbf{r}) = \sum_i |\psi_i^{\text{KS}}(\mathbf{r})|^2. \quad (2.70)$$

We used the superscript KS to remind ourselves that the system we solve is no longer the true system but the non-interacting system. The Kohn-Sham orbitals  $\psi_i^{\text{KS}}$  for example do not necessarily match any physical orbitals of the original system.

Equations (2.67) through (2.69) are the Kohn-Sham equations and from them we can obtain the ground state density. Note however that again our Hamiltonian depends on  $n$  and  $n$  depends on the solution of the equation with our Hamiltonian. This interdependence of the variables implies that the Kohn-Sham equations require a similar self-consistent field approach as the Hartree-Fock equations did.

What we gained by the Kohn-Sham equations compared to for example the Hartree-Fock method is easier computation (no exchange integrals) and an, in principle, exact method to compute the ground state [21]. If the functional  $E_{\text{xc}}$  is known exactly the Kohn-Sham equations give us the exact solution. Unfortunately the exact form of the exchange-correlation functional is not known. Therefore in order to solve the Kohn-Sham equations we need approximations of  $E_{\text{xc}}$ .

### 2.2.3 Exchange-Correlation Functionals

The exchange-correlation functional is the only part in the Kohn-Sham equations that is approximated. Therefore the accuracy of the Kohn-Sham method depends on the accuracy of the exchange-correlation functional. A large number of different exchange-correlation functionals have been developed. The different functionals can be ordered in what Perdew called Jacob's ladder of functionals [23]. In Figure 2.4 we have partly reproduced this ladder.

The ladder starts from the Local Density Approximation (LDA) in which the exchange and correlation are taken from the homogeneous electron gas and the assumption is made that it can be used locally for a density  $n(\mathbf{r})$ . The next level is the Generalized Gradient Approximation (GGA) which besides the local density also uses its derivative to approximate the exchange-correlation potential. This usually leads to better energy approximations but comes at a higher computational cost. The next step up is the meta-GGA in which even higher order derivatives and the kinetic energy density

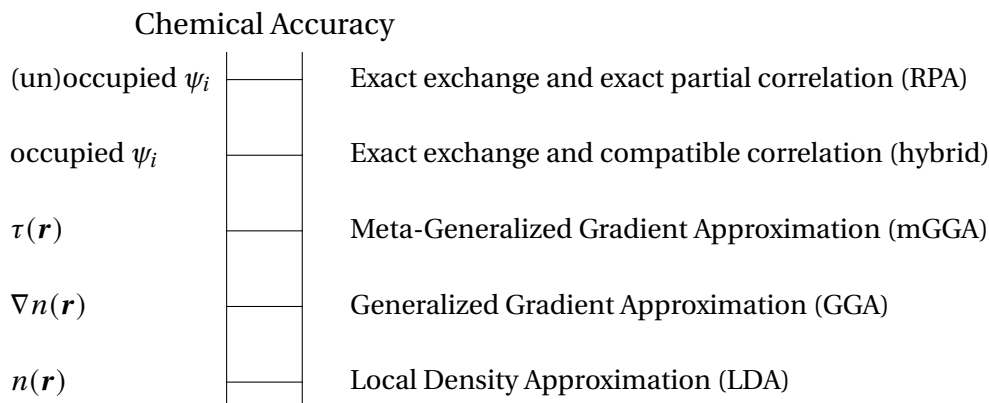


Figure 2.4: Jacob's ladder ordering the different types of exchange-correlation functionals from basic to complex. A partial reproduction of [23].

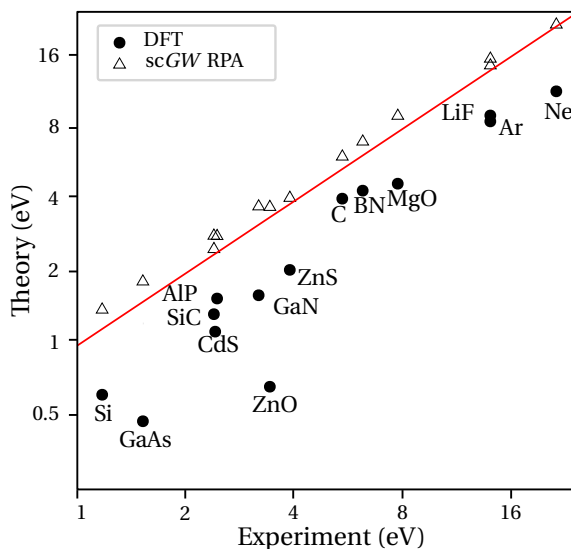


Figure 2.5: Bandgaps obtained from DFT and self consistent GW in the random phase approximation, after Shishkin and Kresse [26].

$\tau$  are included in the approximation. In the last two levels the exchange-correlation is no longer only approximated by the local density and its derivatives but also the Kohn-Sham orbitals are used in the approximation, these type of functionals are called hybrid functionals. They use the orbitals for example to mix in the exact Hartree-Fock exchange. The hybrid functionals lead in general to good results but come at a significant computational cost since they are non-local. Two examples of often used hybrid functionals are B3LYP [24] and PBE0 [25].

## 2.3 Excited States via GW-BSE

Density Functional Theory gives us a good approximation to the ground state of a many-electron system. There is however an infamous limitation to DFT that is called the band-gap problem [27]. An important quantity for the computation of spectra is the band gap, the distance between the lowest unoccupied molecular orbital (LUMO) and the highest occupied molecular orbital (HOMO). DFT underestimates this gap by a large amount, see for example Figure 2.5, in particular function-

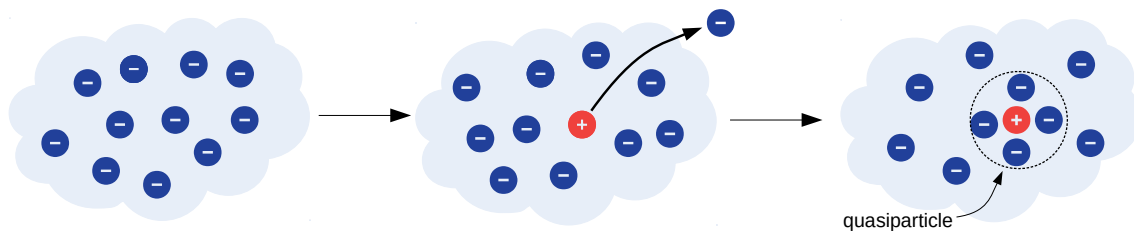


Figure 2.6: The formation of a quasiparticle due to removal of an electron from the system.

als without exact exchange perform terrible. Hence a different theory is needed to correct for this underestimation and this is where the *GW* part of *GW*-BSE comes in. A *GW* calculation gives us a correction to the molecular orbital energies obtained from the Kohn-Sham method that leads to better band gap estimation, see Figure 2.5. The BSE part of *GW*-BSE is then used to describe (neutral) two-particle excitations, like singlets and triplets.

The *GW* calculations are based around the idea of quasiparticles that we present first. Then we present the *GW* method and finally we have a look at the Bethe Salpeter Equations (BSE) for two-particle excitations. In the following we will use second quantization, a reformulation of quantum mechanics in occupation numbers instead of wavefunctions. In the DFT section we represented a quantum state by its wave function  $|\Psi\rangle$  (first quantization) from now on we will also use occupation numbers,  $|N\rangle$  represents a quantum state with  $N$  particles. Second quantization entails more than just a number representation, but a full discussion lies outside the scope of this thesis. More details can be found in [28] and [29].

Furthermore to keep everything relatively simple we restrict ourselves to a spin-singlet and closed-shell (i.e. the total spin is zero) system. These assumptions allow us to neglect spin in our discussions. Furthermore we avoid formal details of most derivations, the interested reader can find a full and formal discussion in [12]. The discussion that follows is mostly based on [30] and [31].

### 2.3.1 Single Particle Excitations, the *GW* Method

Single-particle excitations are excitations where either an electron is removed from a system ( $|N\rangle \rightarrow |N-1\rangle$ ) or added ( $|N\rangle \rightarrow |N+1\rangle$ ) (i.e. they are charged excitations). The removal or addition of an electron to the system gives rise to a quasiparticle. In Figure 2.6 we present the main idea. If we excite a state of  $N$  electrons by removing an electron we leave the system with a positive charge, a hole. The other electrons will rearrange themselves around the hole and effectively screen the interaction of other electrons with the positive charge. The hole plus the layer of negativity surrounding it is called a quasiparticle, in this particular case a quasihole.

These quasiparticles can be described by the one-particle Green's function (the  $G$  in *GW*)

$$G_1(\mathbf{r}, \mathbf{r}', t - t') = -i \langle N, 0 | \hat{T} [\hat{\psi}(\mathbf{r}, t) \hat{\psi}^\dagger(\mathbf{r}', t')] | N, 0 \rangle \quad (2.71)$$

where  $\hat{T}$  is the time-ordering operator and  $\hat{\psi}$  and  $\hat{\psi}^\dagger$  are the annihilation and creation field operators for electrons and  $|N, s\rangle$  is an  $N$ -electron state in the  $s$ -th excited state. For  $t > t'$  this Green's function can be interpreted as the creation of an extra electron at time  $t'$  and position  $\mathbf{r}'$  and the subsequent deletion of the electron at time  $t$  and position  $\mathbf{r}$ . For  $t' > t$  the particle that is created is a hole (electron annihilation). The Green's function describes how the quasiparticle propagates through the system and is therefore called the propagator.

Via a Fourier transform the Green's function can be expressed in terms of frequency or energy instead of time, i.e.  $G_1(\mathbf{r}, \mathbf{r}', \varepsilon)$ . It obeys a Dyson-type equation

$$[\hat{h}_0 + \hat{\Sigma}(\varepsilon)] G_1(\mathbf{r}, \mathbf{r}', \varepsilon) = E G_1(\mathbf{r}, \mathbf{r}', \varepsilon), \quad (2.72)$$

with  $\hat{h}_0 = -1/2\nabla^2 + V_{\text{ext}} + V_{\text{Hartree}}$  and  $\Sigma$  the self-energy. The self-energy takes a similar role as the exchange-correlation functional in DFT, it contains all electron-electron interaction terms. Moreover if one would substitute  $V_{\text{xc}}$  for  $\Sigma$  one would arrive back at DFT. An exact solution to equation (2.72) can be obtained from the Hedin's set of coupled integro-differential equations [32]. The exact solution is however intractable and therefore an approximation is made, the *GW*-approximation, in which the self-energy is

$$\Sigma_{GW}(\mathbf{r}, \mathbf{r}', \varepsilon) = \frac{i}{2\pi} \int G_1(\mathbf{r}, \mathbf{r}', \varepsilon + \varepsilon') W(\mathbf{r}, \mathbf{r}', \varepsilon') d\varepsilon'. \quad (2.73)$$

This self-energy can be interpreted as the energy corresponding to the response of the system on the presence of the particle [33].  $W = \varepsilon^{-1} v_c$  is the screened Coulomb interaction, where  $v_c(\mathbf{r}, \mathbf{r}') = 1/|\mathbf{r} - \mathbf{r}'|$  and  $\varepsilon^{-1}$  is the inverse dielectric function that accounts for the screening and is calculated in the Random-Phase Approximation (RPA) [34]. Using this approximation and rewriting (2.72) in a wavefunction form we arrive at

$$\left[ \hat{h}_0 + \hat{\Sigma}(\varepsilon_i^{\text{QP}}) \right] |\psi_i^{\text{QP}}\rangle = \varepsilon_i^{\text{QP}} |\psi_i^{\text{QP}}\rangle \quad (2.74)$$

where  $|\psi_i^{\text{QP}}\rangle$  are the quasiparticle wave functions and  $\varepsilon_i^{\text{QP}}$  the one particle excitation energies. Note that in practice [30] the quasiparticle wavefunctions are expanded in a basis of Kohn-Sham orbitals, i.e.  $|\psi_i^{\text{QP}}\rangle = \sum c_{ij} |\psi_j^{\text{KS}}\rangle$ . The Hamiltonian can then be expressed as  $\hat{h}_0 = \hat{H}^{\text{KS}} - \hat{V}_{\text{xc}}$ . If we diagonalize the quasiparticle Hamiltonian in the Kohn-Sham basis

$$H_{ij}^{\text{QP}}(E) = \varepsilon_i^{\text{KS}} \delta_{ij} + \langle \psi_i^{\text{KS}} | \hat{\Sigma}(E) - \hat{V}_{\text{xc}} | \psi_j^{\text{KS}} \rangle \quad (2.75)$$

we obtain the quasiparticle energies and states. We can evaluate the quasiparticle energies perturbatively if the off-diagonal elements of the quasiparticle Hamiltonian are small

$$\varepsilon_i^{\text{QP}} = \varepsilon_i^{\text{KS}} + \langle \psi_i^{\text{KS}} | \hat{\Sigma}(\varepsilon_i^{\text{QP}}) - \hat{V}_{\text{xc}} | \psi_i^{\text{KS}} \rangle. \quad (2.76)$$

To solve this equation different methods are used. In the  $G_0W_0$  approach the equation is solved using a Newton fixed point method. This method is also called a one-shot approach since we do not solve the equations self-consistently but assume that one iteration gives a good enough correction to the Kohn-Sham energies to obtain the quasiparticle energies. An improvement of the  $G_0W_0$  is the *evGW* approach in which the quasiparticle energies are updated in the Green's function and the dielectric function until eigenvalue (ev) self-consistency is reached.

The *GW*-approximation gives us a correction to the Kohn-Sham energies. The Kohn-Sham energies are not physical in the sense that they are just Lagrange multipliers. What *GW* does is adding a correction that makes the Kohn-Sham energies physical by introducing the interaction of the particle (electron or hole) with its environment via the quasiparticle picture. This results in a more physical interaction than the exchange-correlation function provides in DFT. Note that this DFT exchange-correlation contribution is actually cancelled in equation (2.76) since it is now contained in the self-energy.

### 2.3.2 Two Particle Excitations, the Bethe Salpeter Equation

Neutral excitations are excitations where the total number of electrons remains constant  $|N, 0\rangle \rightarrow |N, S\rangle$ . These excitations consist of two particles an electron and hole that interact. To study the two particle excitations the two particle Green's function and its Dyson-like equation of motion the Bethe-Salpeter equation (BSE) are investigated [35]. The electron-hole amplitudes of the two particle excitations are

$$\chi_S(\mathbf{x}, \mathbf{x}') = \langle N, 0 | \psi^\dagger(\mathbf{x}') \psi(\mathbf{x}) | N, S \rangle \quad (2.77)$$

To evaluate the BSE these electron-hole amplitudes can be transformed from continuous variables to the basis of single-particle wavefunctions [31]

$$\chi_S(\mathbf{x}, \mathbf{x}') = \sum_v^{\text{occ}} \sum_c^{\text{empty}} A_{vc}^S \psi_c(\mathbf{x}) \psi_v^*(\mathbf{x}') + B_{vc}^S \psi_v(\mathbf{x}) \psi_c^*(\mathbf{x}'). \quad (2.78)$$

Note that the first sum runs over all occupied states ( $v$ ) and the other only over unoccupied ( $c$ ). With this basis the BSE can be rewritten as a generalized eigenvalue problem or two-particle Hamiltonian problem

$$\begin{pmatrix} \mathbf{H}^{\text{res}} & \mathbf{K} \\ -\mathbf{K} & -\mathbf{H}^{\text{res}} \end{pmatrix} \begin{pmatrix} \mathbf{A}^S \\ \mathbf{B}^S \end{pmatrix} = \Omega_S \begin{pmatrix} \mathbf{A}^S \\ \mathbf{B}^S \end{pmatrix}, \quad (2.79)$$

where  $\mathbf{H}^{\text{res}}$  and  $\mathbf{K}$  are

$$H_{vc,v'c'}^{\text{res}} = D_{vc,v'c'} + \kappa K_{vc,v'c'}^x + K_{vc,v'c'}^d, \quad (2.80)$$

$$K_{cv,v'c'} = \kappa K_{cv,v'c'}^x + K_{vc,v'c'}^d \quad (2.81)$$

where  $\kappa = 2$  for singlets and 0 for triplets,

$$K_{vc,v'c'}^x = \int \psi_c^*(\mathbf{r}_e) \psi_v(\mathbf{r}_e) v_c(\mathbf{r}_e, \mathbf{r}_h) \psi_{c'}(\mathbf{r}_h) \psi_{v'}^*(\mathbf{r}_h) d^3\mathbf{r}_e d^3\mathbf{r}_h, \quad (2.82)$$

$$K_{vc,v'c'}^d = - \int \psi_c^*(\mathbf{r}_e) \psi_{c'}(\mathbf{r}_e) W(\mathbf{r}_e, \mathbf{r}_h, \omega = 0) \psi_v(\mathbf{r}_h) \psi_{v'}^*(\mathbf{r}_h) d^3\mathbf{r}_e d^3\mathbf{r}_h. \quad (2.83)$$

$K^x$  is the exchange interaction between the electron and hole and is responsible for the triplet and singlet splitting.  $K^d$  is the direct interaction between the electron and hole, it is the attractive but screened interaction that leads to the electron-hole binding. It is assumed that the dynamic properties of  $W(\omega)$  are negligible and therefore the computationally less demanding approximation  $\omega = 0$  is made [36].

### 2.3.3 Optical Spectra

One of the more important measurable quantities in experiments is the optical spectrum of a material. As we have seen in Chapter 1 the intensity of peaks in the spectrum are given by the oscillator strengths

$$f = \frac{2}{3} \langle \Psi_f | \hat{\mathbf{r}} | \Psi_i \rangle^2 \Omega_S. \quad (2.84)$$

They require the computation of the electric dipole moment  $\langle \Psi_f | \hat{\mathbf{r}} | \Psi_i \rangle$ . They can be calculated from the results of the BSE according to

$$\langle N, S | \hat{\mathbf{r}} | N, 0 \rangle = \sqrt{2} \sum_{vc} A_{vc}^i \langle \psi_c | \hat{\mathbf{r}} | \psi_v \rangle. \quad (2.85)$$

for transitions from the ground state. The sum is taken over all pairs of occupied and unoccupied states. The transition dipole moment between excited states is given by

$$\langle N, S_i | \hat{\mathbf{r}} | N, S_j \rangle = V + C \quad (2.86)$$

$$V = \sum_{vv'} \sum_c D_{vc}^i D_{v'c}^j \langle \phi_v | \hat{\mathbf{r}} | \phi_{v'} \rangle \quad (2.87)$$

$$C = \sum_{cc'} \sum_v D_{vc}^i D_{vc'}^j \langle \phi_c | \hat{\mathbf{r}} | \phi_{c'} \rangle. \quad (2.88)$$

with  $D_{vc}^i = A_{vc}^i - B_{vc}^i$ . For a full derivation of these expressions see Appendix A.

## 2.4 Excited States via TDDFT

An alternative to the  $GW$ -BSE approach is Time-Dependent DFT (TDDFT). In general it is less accurate than the  $GW$ -BSE approach but also less computationally demanding [37]. In this thesis we will use TDDFT only for open shell species (molecules with an unpaired electron), for the practical reason that an implementation of the  $GW$ -BSE method for open shell species was not available at the time of writing. In this section we will give a short overview of the main components of TDDFT for a full discussion see [38].

### 2.4.1 Runge-Gross Theorem and Time-Dependent Kohn Sham Equations

TDDFT has a lot of similarities with normal DFT. In DFT we had the Hohenberg-Kohn theorem (Theorem 1) that states that any observable can be computed from the density  $n(\mathbf{r})$ , TDDFT has a similar theorem the Runge-Gross Theorem [39]:

**Theorem 3** (Runge-Gross). *Two densities  $n(\mathbf{r}, t)$  and  $n'(\mathbf{r}, t)$  starting with the same initial state  $\Psi(t_0)$  under the influence of two different external potentials  $v(\mathbf{r}, t)$  and  $v'(\mathbf{r}, t)$ , both Taylor-expandable around  $t_0$  and differing by only a time-dependent function  $c(t)$  become different infinitesimally later than  $t_0$ .*

This theorem implies that once again the (time-dependent) density is enough to determine the state of a system. Which implies that any observable is a unique functional of the time-dependent electron density and the initial state. It was also proven that, similar to the Kohn-Sham equations, for any interacting electron system, there exists another non-interacting electron system (with another external potential) with the same density [40]. With this result we can construct the time-dependent Kohn-Sham equations

$$i \frac{\partial}{\partial t} \psi_i^{\text{KS}}(\mathbf{r}, t) = \left[ -\frac{1}{2} \nabla^2 + v_s[n](\mathbf{r}, t) \right] \psi_i^{\text{KS}}(\mathbf{r}, t), \quad (2.89)$$

with the single-particle potential given by

$$v_s[n](\mathbf{r}, t) = v_0(\mathbf{r}, t) + \int \frac{n(\mathbf{r}', t)}{|\mathbf{r} - \mathbf{r}'|} d\mathbf{r}' + V_{\text{xc}}(\mathbf{r}, t). \quad (2.90)$$

Also in TDDFT all the difficult parts are collected in the exchange-correlation function  $V_{\text{xc}}$ , only now it also depends on time. Similar to DFT the accuracy of TDDFT is highly dependent on the accuracy of the chosen exchange correlation functional.

### 2.4.2 Excitations

To find excitations from TDDFT one studies the density response of a system to an external time-dependent perturbation and generally in an explicitly spin-dependent formulation [41]. The spin-density response is

$$n_{1\sigma}(\mathbf{r}, \omega) = \sum_{\sigma'} \int \chi_{s,\sigma\sigma'}(\mathbf{r}, \mathbf{r}', \omega) v_{s1\sigma'}(\mathbf{r}', \omega) d\mathbf{r}', \quad (2.91)$$

with the effective potential

$$v_{s1\sigma}(\mathbf{r}, \omega) = v_{1\sigma}(\mathbf{r}, \omega) + \sum_{\sigma'} \int f_{\text{Hxc},\sigma\sigma'}(\mathbf{r}, \mathbf{r}', \omega) n_{1\sigma'}(\mathbf{r}', \omega) d\mathbf{r}', \quad (2.92)$$

where  $v_{1\sigma}$  is the perturbing potential and

$$f_{\text{Hxc},\sigma\sigma'}(\mathbf{r}, \mathbf{r}', \omega) = \frac{1}{|\mathbf{r} - \mathbf{r}'|} + f_{\text{xc},\sigma\sigma'}(\mathbf{r}, \mathbf{r}', \omega) \quad (2.93)$$

where  $f_{xc,\sigma\sigma'}(\mathbf{r}, \mathbf{r}', \omega)$  is the functional derivative of the exchange-correlation functional with respect to the density. Furthermore the Kohn-Sham response is given by

$$\chi_{s,\sigma\sigma'}(\mathbf{r}, \mathbf{r}', \omega) = \delta_{\sigma\sigma'} \sum_{j,k=1}^{\infty} (f_{k\sigma} - f_{j\sigma}) \frac{\psi_{j\sigma}(\mathbf{r})\psi_{k\sigma}^*(\mathbf{r})\psi_{j\sigma}^*(\mathbf{r}')\psi_{k\sigma}(\mathbf{r}')}{\omega - \omega_{jk\sigma} + i\eta}, \quad (2.94)$$

where  $\eta$  is an infinitesimally small number. Note that the sum runs over all pairs of occupied and unoccupied pairs. If both are occupied their contribution is zero to the sum.

Combining these results we obtain for the spin-density response

$$n_{1\sigma}(\mathbf{r}, \omega) = \sum_{\sigma'} \int \chi_{s,\sigma\sigma'}(\mathbf{r}, \mathbf{r}', \omega) \left[ v_{1\sigma}(\mathbf{r}, \omega) + \sum_{\sigma''} \int f_{\text{Hxc},\sigma\sigma'}(\mathbf{r}', \mathbf{r}'', \omega) n_{1\sigma''}(\mathbf{r}'', \omega) d\mathbf{r}'' \right] d\mathbf{r}'. \quad (2.95)$$

Exact excitation energies are obtained from the poles of the density-density response function [41]. However no perturbation is necessary, a system sustains a finite response at its excitation frequencies. And the corresponding eigenmodes and eigenfrequencies can be obtained from the eigenvalue equation

$$n_{1\sigma}(\mathbf{r}, \Omega) = \sum_{\sigma'} \int \chi_{s,\sigma\sigma'}(\mathbf{r}, \mathbf{r}', \Omega) \sum_{\sigma''} \int f_{\text{Hxc},\sigma\sigma'}(\mathbf{r}', \mathbf{r}'', \Omega) n_{1\sigma''}(\mathbf{r}'', \Omega) d\mathbf{r}'' d\mathbf{r}'. \quad (2.96)$$

This last equation can be cast into a generalized eigenvalue problem known as the Casida equation [42, 43]

$$\begin{pmatrix} \mathbf{A}(\omega) & \mathbf{B}(\omega) \\ \mathbf{B}^*(\omega) & \mathbf{A}^*(\omega) \end{pmatrix} \begin{pmatrix} \mathbf{X} \\ \mathbf{Y} \end{pmatrix} = \Omega \begin{pmatrix} 1 & 0 \\ 0 & -1 \end{pmatrix} \begin{pmatrix} \mathbf{X} \\ \mathbf{Y} \end{pmatrix}, \quad (2.97)$$

where

$$A_{ia,jb}(\omega) = \delta_{ij} \delta_{ab} \varepsilon_{ai} + (ia|f_{\text{Hxc}}(\omega)|jb) \quad (2.98)$$

$$B_{ia,bj}(\omega) = (ia|f_{\text{Hxc}}(\omega)|bj) \quad (2.99)$$

and

$$(pq|f|rs) = \iint \psi_p^*(1)\psi_q f(1,2)\psi_r^*(2)\psi_s(2) d1 d2. \quad (2.100)$$

From this the excitation energies  $\Omega$  can be obtained. It is very similar to the generalized eigenvalue problem of the BSE and gives us the same information, i.e. we can identify  $\mathbf{X}$  and  $\mathbf{Y}$  with the matrices  $\mathbf{A}$  and  $\mathbf{B}$  of the generalized eigenvalue problem obtained from the BSE.

## Chapter 3

# Exciton and Charge Carrier Dynamics in Disordered Organic Molecular Systems

In Section 1.1.1 we described the basic ideas of how charge transport in disordered organic molecular systems takes place. Charges are localized and can hop, via a quantum mechanical tunnelling process, from localized site to site, where a site can either be a molecule or part of a molecule. Besides charges, also excitons move according to a hopping process, the basic physics of electron, hole and exciton hopping is the same.

In this chapter we discuss the modelling of carrier (electron, hole and exciton) dynamics in more detail. We start by discussing the most basic model that only accounts for hopping of a single carrier and the main approach to solving it, the Master Equation (ME) approach. From there we build towards more advanced models and introduce different carrier types and more processes. We will see that the ME approach is too limited to account for all dynamical processes and a different method, the kinetic Monte Carlo (KMC) method, is introduced. At the end of the chapter we give an overview of how all parameters can be obtained.

### 3.1 The Hopping Model

The main process underlying the hopping model is a single hop between two sites. This is a bimolecular charge transfer process that is often described by either the Miller-Abraham's rate [44]

$$v_{ij} = \begin{cases} v_0 \exp\left(-2\alpha R_{ij} - \frac{\Delta E_{ij}}{k_B T}\right) & \Delta E_{ij} > 0 \\ v_0 \exp(-2\alpha R_{ij}) & \Delta E_{ij} \leq 0 \end{cases}, \quad (3.1)$$

or the Marcus rate [45]

$$v_{ij} = \frac{2\pi}{\hbar} \frac{|J_{ij}|^2}{\sqrt{4\pi\lambda_{ij}k_B T}} \exp\left(-\frac{(\Delta E_{ij} + \lambda_{ij})^2}{4\lambda_{ij}k_B T}\right). \quad (3.2)$$

$\Delta E_{ij} = E_j - E_i$  is the energy difference between the two sites,  $R_{ij}$  the distance,  $\alpha$  is called the inverse localization length and indicates how spread out the wave function of a site is and  $v_0$  is the attempt frequency.  $J_{ij}$  is the electronic coupling element between sites  $i$  and  $j$  and  $\lambda_{ij}$  is the reorganization energy associated with a hop.

These last two parameters are also the main difference between the Miller-Abraham's and Marcus rate. The Marcus rate takes the coupling between sites explicitly into account and accounts for the reorganization energy of the sites (the energy associated with the structural change due to the presence of a carrier). It is important to realize that the parameters in the rate equations are carrier type dependent, e.g. an electron has a different localization length than a hole, a different site energy etc.

The hopping rates indicate how likely it is that a carrier will hop from one site to another. To model the full material we also need to describe the sites or system morphology. For the sites often

the center of mass of the molecules is taken as the location of a site. All other parameters of a site, such as the site energy and reorganization energy can be computed from the electronic structure calculations discussed in Chapter 2 and some classical simulation methods.

To turn the rates and sites into a model that describes charge transport we consider the material as a weighted directed graph. We identify the site  $i$  with a vertex and the rate  $v_{ij}$  with a weighted and directed edge from site  $i$  to site  $j$ . For a single carrier the state of the system is fully described by the location  $i$  of the carrier. The hopping of the carrier can now be seen as a Markovian stochastic process and a powerful tool exists to solve the dynamics of this process, the Master Equation (ME).

### 3.1.1 The Master Equation

The master equation is a differential form of the Chapman-Kolmogorov equation for Markovian stochastic processes. It describes the evolution of the occupation probability for a discrete set of states. For a comprehensive derivation of the master equation from the Chapman-Kolmogorov equation the reader is referred to [46]. Here we will state the master equation in its most basic form

$$\frac{dp_i}{dt} = \sum_{j \neq i} [W_{ij}p_j - W_{ji}p_i]. \quad (3.3)$$

The indices  $i$  and  $j$  represent possible states of the system and the  $p_i$  the probability of occupation of state  $i$ ,  $W_{ij}$  is the transition rate from  $j$  to  $i$  (i.e.  $v_{ji}$ ).

In general the master equation can be interpreted as the sum of the probability flow into a state  $i$ ,  $\sum_{j \neq i} W_{ij}p_j$ , and the flow out of that state,  $\sum_{j \neq i} -W_{ji}p_i$ . Note that this last sum can be rewritten as  $\sum_{j \neq i} -W_{ji}p_i = W_{ii}p_i$ , with  $W_{ii} = -\sum_{j \neq i} W_{ji}$ , resulting in the most compact form of the master equation

$$\frac{d\vec{p}}{dt} = W\vec{p}, \quad (3.4)$$

where  $\vec{p}$  is the vector containing all  $p_i$ 's and  $W$  a matrix where the  $i, j$ th entry is given by  $W_{ij}$ .

### 3.1.2 The Master Equation for a Single Carrier

The ME for a single carrier is

$$\frac{dp_i}{dt} = \sum_{j \neq i} [p_j v_{j \rightarrow i} - p_i v_{i \rightarrow j}], \quad (3.5)$$

where  $p_i$  is the occupation probability of site  $i$  (and hence state  $i$ ) and  $v_{i \rightarrow j}$  is the hopping rate from site  $i$  to site  $j$ . A stationary solution to the system is easily found using linear algebra techniques especially when the compact form of the master equation (3.4) is used.

What the stationary solution gives is the average occupation of a site and from these occupations other properties like the carrier mobility can be derived. In general we have for an observable  $O$  with value  $O_i$  in state  $i$

$$\langle O \rangle = \sum_i O_i p_i. \quad (3.6)$$

Using this equation most interesting material properties can be derived.

### 3.1.3 The Master Equation for Multiple Carriers

The ME for a single carrier is useful only for a material where the carrier density is almost zero, i.e. the carrier does not meet any other carrier while hopping around. In a real material multiple carriers are present and carriers repel one another, e.g. the probability of finding two electrons on the same

site is zero due to their Coulomb repulsion. This effect is known as the *site exclusion effect* where no two carriers of the same type can occupy the same site.

To describe the state of a system with multiple carriers we use site occupation numbers

$$\{n\} = \{n_1, n_2, \dots\}, \quad n_i \in \{0, 1\}, \quad (3.7)$$

where each  $n_i$  indicates whether or not site  $i$  is occupied. Note, for  $N$  particles in the system we have  $\sum_i n_i = N$ . The basic master equation for this system is

$$\frac{dp_{\{n\}}}{dt} = \sum_{\{m\} \neq \{n\}} [W_{\{n\}\{m\}} p_{\{m\}} - W_{\{m\}\{n\}} p_{\{n\}}]. \quad (3.8)$$

This set of equations gets very large due to the large size of the state space, for  $M$  sites the state space has a size of  $\binom{M}{N}$ , therefore a switch is made to average site occupations  $f_i$ , as suggested by [47],

$$f_i = \sum_{\{m\}} m_i p_{\{m\}}. \quad (3.9)$$

To convert the rates we need to make more assumptions. Firstly we assume that only one particle hops at the same time, furthermore hops can only occur between an occupied and an unoccupied site (the site exclusion from earlier). The only allowed transitions are then transitions from  $\{n\} \rightarrow \{m\}$  such that

$$n_i = m_i \quad \forall_{i \notin \{r,s\}}; \quad n_r = 0 \quad n_s = 1; \quad m_r = 1 \quad m_s = 0. \quad (3.10)$$

Or in words: only single particle hops from site  $s$  to site  $r$ , where site  $s$  was occupied and  $r$  was unoccupied, are allowed. The probability that site  $r$  is not occupied and  $s$  is, is given by  $f_s(1 - f_r)$ . Then the total rate for the hop from  $s$  to  $r$  is given by  $W_{rs} f_s(1 - f_r)$  and we arrive at what is called the Pauli Master Equation,

$$\frac{df_i}{dt} = \sum_{j \neq i} [W_{ij} f_j(1 - f_i) - W_{ji} f_i(1 - f_j)] \quad (3.11)$$

$$= \sum_{j \neq i} [v_{j \rightarrow i} f_j(1 - f_i) - v_{i \rightarrow j} f_i(1 - f_j)]. \quad (3.12)$$

Note however that this equation is no longer a master equation in the mathematical sense due to the non-linearity in  $f$ . Furthermore the  $v_{i \rightarrow j}$ 's are calculated from hopping rates and not from the original rates of the Markov process.

It is important to note that the Pauli Master Equation is a dependent set of nonlinear equations, hence an infinite number of stationary solutions exist. To solve this problem an extra equation is needed that fixes the number of carriers  $N$  in the system [48],

$$\sum_i f_i = N. \quad (3.13)$$

Due to the non-linearity of equation (3.12) solving it is no longer straightforward and different methods are used, a brief overview of the most used methods is given in Appendix B.1.

## 3.2 Extending the Hopping Model

The hopping model and master equation give us a good model to describe the dynamics of multiple carriers of the same type in a disordered organic material. We are however also interested in dynamics with multiple carrier types, e.g. the dissociation of singlets into free charges via CT-states.

In principle a full ME could be set up for this problem, but the state space is even larger than that for the multiple carrier case. Furthermore a reduction of the state space to average site occupations is no longer possible since transitions of carrier types (e.g. free charges forming an exciton) can not be modelled as a simple hop from site to site. This makes the ME approach practically infeasible (although recently an attempt has been made to extend the ME approach with generation and recombination of charges, see Appendix B.2).

Instead a kinetic Monte Carlo (KMC) approach is used. KMC is a brute force method, instead of trying to solve balance equations such as the ME, the KMC approach computes different trajectories through the state space by explicitly simulating the dynamics of the material. A KMC simulation starts from an initial state, from there all possible transitions (events) to other states are computed. An event is selected based on the rate (likelihood) and the state is updated, then again all possible transitions to other states are computed, one is selected etc. In this way a trajectory is computed.

The main advantage of KMC is that we no longer need to consider the complete state space but only the part that is relevant for the next possible events. Furthermore as long as a transition from one state to another can be described by a rate we can add it to the simulation without difficulty. We will now repeat the list of all the processes relevant for organic electronics presented in Section 1.1.3, but with their corresponding rates. Thereafter we present the full KMC algorithm.

### 3.2.1 Charge Transfer

The main process in the KMC model is the transfer of charge carriers that we discussed before. In this thesis we will use the Marcus rate to describe the charge transfer.

### 3.2.2 Exciton Transfer

For exciton hopping multiple rates exist, the Förster rate, Dexter and Marcus rate are three examples. The Förster rate is used to describe long range hopping via virtual photon exchange [49]. It is mostly relevant for hopping of singlets since they can emit a virtual photon, triplets can not. The Förster rate is an adaptation of the Miller-Abraham's rate

$$v_{ij} = \begin{cases} v_0 \left(\frac{a}{R_{ij}}\right)^6 \exp\left(-\frac{\Delta E_{ij}}{k_B T}\right) & \Delta E_{ij} > 0 \\ v_0 \left(\frac{a}{R_{ij}}\right)^6 & \Delta E_{ij} \leq 0 \end{cases}, \quad (3.14)$$

where  $a$  is the Förster radius and is an indication of how far the singlet can hop. Dexter transfer is relevant for triplet transport and is based on electron exchange between two sites [50]. Electron transfer is a short range process and depends on the localization length of the wavefunctions, therefore the rate is identical to the Miller-Abraham's rate only the values of the parameters differ.

An alternative approach to the Dexter and Förster type rates is again the Marcus rate, equation (3.2), where the coupling between sites is computed explicitly. This is the approach taken in this thesis.

### 3.2.3 Exciton Generation

Exciton generation is modelled as a special case of charge carrier hopping and occurs if either an electron hops onto a site with a hole or if a hole hops to a site with an electron. Since it is difficult to obtain reorganization energies for these processes, the Miller-Abraham's rates are used to describe this process, equations (3.1), where the energy difference now includes the binding energy of the exciton, i.e.  $\Delta E_{\text{gen},ij} = E_j - E_i - E_b$ , with  $E_b$  the binding energy of the exciton.

### 3.2.4 Exciton Dissociation

Excitons can also dissociate, a widely used model for exciton dissociation is based on an intermediate step, the charge transfer state [51]. The exciton splits in a separate electron and hole that live on two separate molecules, the coulomb interaction keeps them bounded together. This bounded state is called the charge transfer (CT) state. The CT state can then dissociate into free charges. These processes are again modelled by the Miller-Abraham's rates (eq. 3.1) with an adapted energy term.

For the dissociation of an exciton into a CT-state the energy difference is  $\Delta E_{ij} = E_j - E_i + E_b - E_{CT}$ , with  $E_{CT}$  the CT-state binding energy. The binding energy of the CT-state can be approximated with the Coulomb attraction, i.e.  $E_{CT} \approx k_e \frac{1}{R_{ij}}$ , with  $k_e$  the Coulomb constant. For the dissociation of the CT-state to free charges the energy difference is  $\Delta E_{ij} = E_j - E_i + E_{CT}$ .

### 3.2.5 Exciton Decay

Singlet excitons can decay radiatively (by emitting a photon) back to the ground state. The radiative decay time  $\tau_{rad}$ , is obtained from Einstein's formula for spontaneous emission

$$\tau_{rad}^{-1} = \sqrt{\varepsilon} \frac{4\alpha\Omega_S^3}{3c^2\hbar^3} |\boldsymbol{\mu}|^2, \quad (3.15)$$

where  $\varepsilon$  is the dielectric constant of the material,  $\alpha$  the fine structure constant and  $\boldsymbol{\mu}$  the transition dipole between the ground and excited state  $S$ . Besides radiative decay excitons can also decay non-radiatively, these processes are neglected in the current implementation. Nonetheless the radiative decay rate is a lower bound to the full decay rate [52]

$$r_{decay} = \tau_{decay}^{-1} = \tau_{rad}^{-1} + \tau_{nonrad}^{-1} > \tau_{rad}^{-1}. \quad (3.16)$$

### 3.2.6 The Kinetic Monte Carlo Algorithm

The kinetic Monte Carlo algorithm is relatively simple and consists of the following steps [53, 9].

1. **Initialize:** Initialize the system with all parameters and add the initial carriers.
2. **Compute next event rates:** For all possible next events,  $j$ , for all carriers in the simulation, the corresponding rates  $r_j$  need to be calculated. To keep this feasible, in general a cut-off is applied to the distance a carrier can hop. This cut-off distance can be different between species, for example singlet excitons can hop further than electrons and therefore a larger cut-off is applied for singlet excitons than for electrons or holes.
3. **Select next event:** From the possible next events one event is selected. A uniform random number is drawn,  $x \sim \text{Unif}([0, r_T])$ ,  $r_T = \sum_j r_j$ , and the next event  $j$  is given by the  $j$  that satisfies:  $\sum_{k=1}^{j-1} r_k \leq x \leq \sum_{k=1}^j r_k$ .
4. **Event execution:** The event is executed and the time is advanced. If the event is a hop the carrier is moved to the new site, if the event is exciton decay the exciton is deleted etc. To advance the time a random time is drawn from an exponential distribution based on the total rate, i.e.  $\tau \sim \text{Exp}(\frac{1}{r_T})$ , then the time is advanced  $\text{time} = \text{time} + \tau$ . Finally the change is registered to keep track of the system trajectory.
5. **Repeat:** Steps two to four are repeated until a certain end time or number of events has occurred. Since we are interested in transient behaviour this condition is enough. To derive steady state properties from the KMC one needs to repeat the steps until the simulation has converged to the steady state and enough accuracy has been reached.

### 3.3 Material Morphology and Rate Parameter Calculations

To use the KMC or ME approach the system morphology and the parameters used in the rate equations need to be calculated. In this section we present a short overview of their computation, for more details see for example [54] or [55].

#### 3.3.1 Site Locations and Simulation Box

Only a small part of the material is modelled in the KMC model. A small simulation box is chosen that is small enough to make the simulation computationally feasible and large enough to be a representative sample. The locations of the molecules within the simulation box are obtained via Molecular Dynamics (MD) (for example with a software package like GROMACS [56]), the material is frozen in time and the center of masses are used as the locations of the sites in the simulation.

To allow for numerical simplifications and optimizations the sites are sometimes placed on a lattice with spacing  $a$ . The parameter  $a$  is then fitted to experimental data. The argument for this simplification is that in general the energetic disorder of an organic material is larger than the positional disorder [57]. Nonetheless it means that the positional parts of the rate equations (see next section) are just constants, which is a rather rough approximation. We will therefore adopt the model with the site locations obtained from MD such that positional and energetic disorder are both taken into account.

#### 3.3.2 Site Energies

The energy levels of a single molecule are obtained by the many-body approach discussed in Chapter 2. In a material however the molecules experience exchange, dispersion and electrostatic interactions between them that lead to a shift in the energy levels of every molecule. This is referred to as energetic disorder. To compute the energetic disorder we focus on the electrostatic interaction. The reason being that we are interested in energy differences and hence we can ignore interactions that influence both sites almost equally like the dispersion interaction [58]. Furthermore the electrostatic interaction is the strongest interaction and therefore dominates the energy shift. The energy of a molecule in state  $i$  is given by

$$E^i = E_{\text{vac}}^i + E_{\text{corr}}^i, \quad (3.17)$$

where  $E_{\text{vac}}^i$  is the vacuum (single molecule) energy and  $E_{\text{corr}}^i$  the electrostatic correction due to the interaction with surrounding molecules. The calculation of these electrostatic corrections is rather involved and we rely on the VOTCA-XTP package [59, 54, 60] to compute them for us. For details on how the corrections are computed see [55] and [58]. Note that the energies of a site are carrier dependent. The energy corresponding to an electron is the (shifted) LUMO energy of the molecule, for a hole the HOMO energy and for an exciton the corresponding singlet energy.

#### 3.3.3 Reorganization Energies

If charge transfer occurs one molecule changes from an occupied to a neutral state and the other molecule from a neutral to an occupied state. These changes lead to a reorganization of the nuclear coordinates that consume energy, the (intramolecular) reorganization energy  $\lambda_{ij}$ . It is computed from four points on the potential energy surface (PES) of both molecules in the neutral and charged states. For a molecule  $i$  that loses its charge and molecule  $j$  that obtains the charge we have [61]

$$\lambda_{ij} = \lambda_i^{cn} + \lambda_i^{nc} = U_i^{nC} - U_i^{nN} + U_j^{cN} - U_j^{cC}, \quad (3.18)$$

where  $U_i^{nC}$  stands for the energy of molecule  $i$  in state  $n$  and geometry (capital)  $C$ .

### 3.3.4 Electronic Coupling Elements

The electronic coupling elements are given by

$$J_{ij} = \langle \phi^i | \hat{H} | \phi^j \rangle, \quad (3.19)$$

where the  $\phi^i$  and  $\phi^j$  are wave functions corresponding to molecules  $i$  and  $j$  participating in the charge transfer and  $\hat{H}$  is the Hamiltonian of the dimer (i.e. the two molecules together). The value of the transfer integral depends heavily on the configuration of the participating molecules and therefore on the whole morphology [54]. Since  $J_{ij}$  needs to be computed for every pair of molecules an efficient yet accurate method is needed. We have used the DIPRO (dimer projection) approach from [62] for the electrons and holes as implemented in the VOTCA-XTP package. For the excitons we have used the transition charge from electrostatic potential (TrESP) method [63], to reduce the computational cost. A DIPRO method for excitons does exist however [64], but is computationally more demanding.

### 3.3.5 Attempt Frequency and Localization Length

Given the reorganization energies and coupling elements, the first factor of the Marcus rate,  $\frac{2\pi}{\hbar} \frac{|J_{ij}|^2}{\sqrt{4\pi\lambda_{ij}k_B T}}$ , is known. To get approximate values for the inverse localization length and attempt frequency of the electrons and holes used in the Miller-Abraham's rates the first factor of this rate is fitted to the first factor of the Marcus rate. To be a bit more precise the coupling elements are represented as a function of distance  $J_{ij}(R)$  and an exponential function of the form  $Ae^{-B \cdot R}$  is fitted to  $\frac{2\pi}{\hbar} \frac{|J_{ij}(R)|^2}{\sqrt{4\pi\lambda_{ij}k_B T}}$ .  $A$  can then be identified with the attempt frequency  $\nu_0$  and from  $B$  we get the inverse localization length with  $B = 2\alpha$ .

# Chapter 4

## Transient Absorption of a Benzene TCNE Mixture

In this chapter we apply the multiscale model to a model system of TCNE and benzene molecules to simulate the transient absorption spectra. We start by discussing the model system. First we briefly discuss how all computations and simulations were done, next we discuss the results of the parameter calculations, in particular the density of states and rates will be presented. Thereafter we present the simulated carrier dynamics and TAS signal. We will see that the TAS signal can indeed be linked to some of the underlying processes. In the last section of this chapter we present simulations performed with changes to the parameters to investigate their influence on the TAS signal and carrier dynamics.

### 4.1 The Model System

True organic electronic devices consist of many molecules that often have a complex and large structure. This makes simulating these systems computationally very expensive. For the objective of this thesis (linking TAS signals to dynamics) it is not necessary to simulate full devices or materials. Therefore we consider a smaller test system consisting of 3200 TCNE and 3200 benzene molecules (see Figures 2.1 and 1.5b) that is large enough to get interesting dynamics, but small enough to be easily simulated.

In this section we will start by discussing exactly how the computations and simulations were performed for the model system. Thereafter we present an overview of the most important model parameters/results, such as the rates and density of states. This is done to get a feel for what the model system is and how it should behave, which will aid the discussion of the results in the sections that follow. At the end of this section we also briefly discuss the performance and sensitivity of the KMC method.

#### 4.1.1 Computational Methods and Simulation Method

The molecules, 3200 of each type, are put into a  $10 \times 10 \times 10$  nm simulation box with periodic boundary conditions. The number of molecules is chosen such that the density of the material resembles the average density of TCNE and benzene. The morphology of the system is obtained by relaxing the system with constant temperature molecular dynamics using GROMACS [56]. The modified Berendsen thermostat is used to stabilize the system to 300K. For the integration the leap-frog integrator is used with a time step of 0.002fs. The system is simulated for 100ps to let the temperature stabilize. The force field and initial structure of the molecules are obtained from the Automated Topology Builder (ATB) [65, 66]<sup>1</sup>. A part of the morphology is visualized in Figure 4.3.

---

<sup>1</sup>The specific molecules and force fields used; TCNE: molid=40554, hash=c9c27; Benzene: molid=219157, hash=167b6

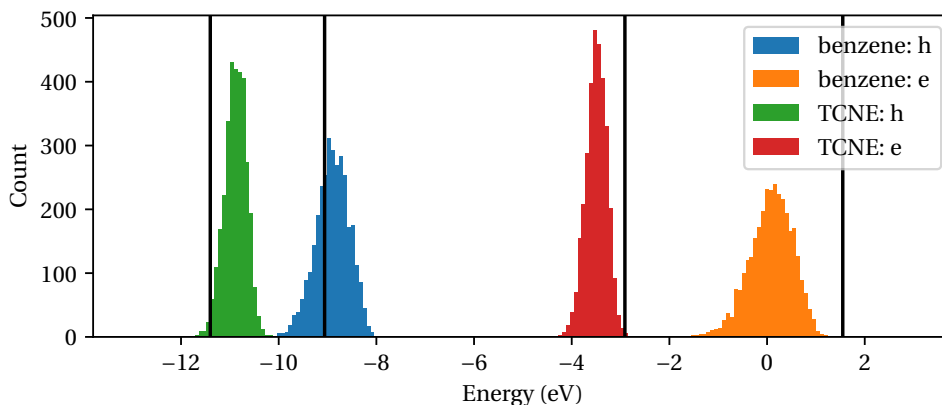


Figure 4.1: The DOS of the TCNE benzene model system. The labels refer to the molecules and the e and h refer to the LUMO and HOMO levels respectively. The black lines are for reference and represent the vacuum energies of the separate molecules.

All electronic structure calculations are performed with the use of the DFT and *GW*-BSE methods implemented in VOTCA-XTP [59, 54, 60], except for the open shell excited states of the cation and anion of the TCNE and benzene molecule, these calculations are performed using the TDDFT implementation of ORCA [67]. For all electronic structure calculations the def2-tzvpd basis set [68] is used and for the DFT calculations the B3LYP functional [24].

To perform the kinetic Monte Carlo simulations the algorithm and processes discussed in Chapter 3 are implemented in C++. <sup>2</sup> The code is currently specifically adapted for the TCNE and benzene model system. Results of the simulations were averaged over 25 runs (trajectories) of 1500ps to obtain the results that are presented in this chapter. In the KMC simulation a cut off (see Section 3.2.6) was used for the possible hops of electrons, holes and singlets. For the electrons and holes a cut off of 0.5 nm was employed and for singlets a cut off of 4.0 nm.

To simulate the pump-probe experiment we excite a certain percentage of the molecules at the start of the KMC simulation (the pump pulse). After that the KMC is used to evolve the system, since we can get the state of the system at every time step, we do not need to simulate the probe pulse. We can just look at the state of the system at a certain time and compute the absorption spectrum from it. From experiments it is known that 0.1 to tens of percents of the molecules get excited due to the pump pulse [7]. We will assume that 10% of the molecules get excited due to the pulse throughout this chapter unless stated otherwise.

The absorption spectra are obtained via an average. First the individual spectra of all the different molecules in their different states (electron, hole etc.) are computed using the electronic structure calculations techniques. Then an average spectrum is taken over all the molecules in their corresponding state. It is assumed that charge transfer states are dark, i.e. do not contribute to the absorption spectra.

#### 4.1.2 The Density Of States

Benzene and TCNE form a so-called donor-acceptor pair. One molecule can donate an electron and the other is able to accept it. This system was specifically chosen for this fact, since it allows for the easy formation of charge transfer states in which a positive and negative charge are on two different molecules.

<sup>2</sup>[www.github.com/rubengerritsen/KMC](http://www.github.com/rubengerritsen/KMC)

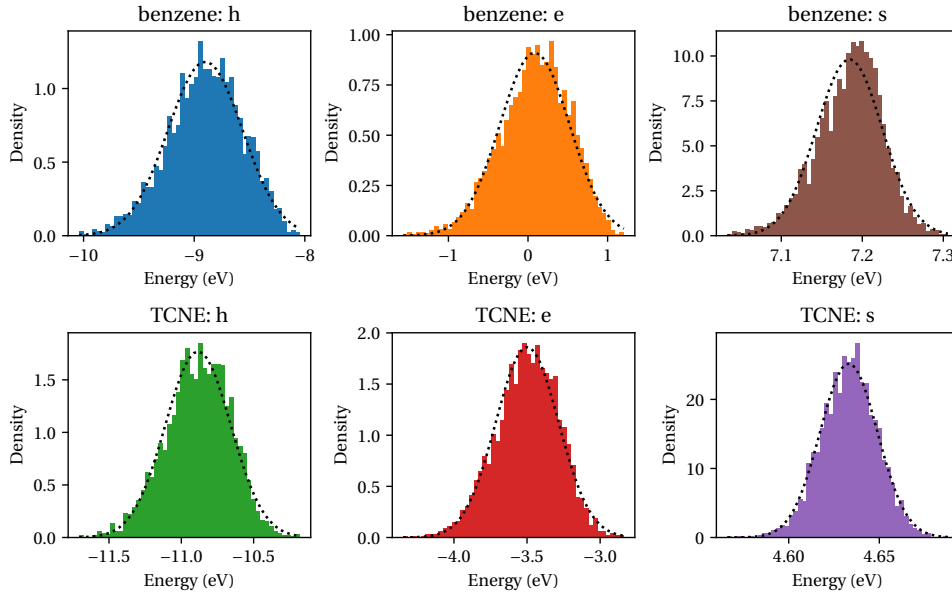


Figure 4.2: The DOS separately for the different carrier types, electrons (e), holes (h) and singlets (s). A normal distribution has been fitted to the DOS (black dotted line), the exact parameters can be found in Table 4.1.

	$E_{\text{vac}}$ (eV)	$\mu$ (eV)	$\sigma$ (eV)
benzene: h	-9.08	-8.9	0.34
benzene: e	1.55	0.08	0.44
benzene: s	7.2	7.18	0.04
TCNE: h	-11.41	-10.88	0.23
TCNE: e	-2.92	-3.5	0.21
TCNE: s	4.59	4.63	0.02

Table 4.1: A summary of the parameters of the normal distributions fitted to the DOS of the model system. Also the vacuum energy levels for the different states are presented for comparison.

The Density of States (DOS) is one of the most important properties for charge and exciton dynamics and the formation of the charge transfer states. The DOS of the model system is presented in Figures 4.1 and 4.2. In Figure 4.1 we see the donor-acceptor behaviour of the system, the LUMO (e) level of TCNE lies lower in energy than the LUMO level of benzene. Hence the TCNE molecule is the acceptor of the electron, since it is energetically more favourable for the electron to be on the TCNE molecule. The benzene molecule is the donor since the HOMO level lies higher in energy and hence it is more likely to carry a positive charge (a hole).

Besides the donor-acceptor behaviour of the system we also see the spread in energy levels due to the electrostatic interaction between the molecules discussed in section 3.3.2. We chose to compute the DOS explicitly, but in many cases a Gaussian DOS is used, in Figure 4.2 we have also fitted a Gaussian to the DOS for comparison, the exact parameters are summarized in Table 4.1. We see that the Gaussian approximation of the DOS is rather accurate. It should, however, be noted that the energy landscape is more complex than just Gaussian distributed, since the molecules influence one another the landscape is correlated, an effect that cannot be seen in figures of the DOS such as Figure 4.2.

### 4.1.3 Processes Visualized

To aid in the following discussions of the processes, dynamics and the corresponding rates of the model system, we present in Figure 4.3 a visual summary of the most important processes involved. We see a singlet in Figure 4.3a, that dissociates into a CT state, Figure 4.3b, and finally separates into free charges, Figure 4.3c and d.

### 4.1.4 Rates

An overview of the rates in the model is presented in Figure 4.4, 4.5 and 4.6. From these figures we see that two different rates have been used. For the normal hopping we have the Marcus rate, but for the dissociation and generation processes we have the Miller-Abraham's rate. The Miller-Abraham's (MA) formalism makes a sharp distinction between hops downward in energy and upward. For downward hops no energy penalty is included and hence we see the exponential decay with distance for hops downward in energy as a thick line of points in the figures, e.g. 4.5b shows almost only hops downward in energy and hence we see the exponential decay with distance of the rate. The points below this line (for the MA rates) are for hops or transitions that are upwards in energy. We see in particular in Figure 4.4c through f that the effect of the energy barrier can be very large and leads to a dramatic reduction of the rates.

Figures 4.4a and b, based on the Marcus rate, can be interpreted along similar lines, the rates in the top part of the point clouds are hops downward in energy and to similar energies and the bottom parts correspond to hops that require more energy.

It should be noted that the large differences between the different rates for hops between different molecules is due to the donor-acceptor behaviour of the system. This becomes extra apparent when we consider for example Figure 4.4c, we see that the rate for hops of an electron from benzene to TCNE is very large and the hop from TCNE to benzene very small. This is exactly as expected since TCNE is the electron acceptor in this system. Similar conclusions can be drawn for all the graphs in Figure 4.4.

Care must be taken when interpreting the rates related to singlet dissociation. In Figures 4.4c through f, for example, the CT dissociation via an electron (figure e) may seem fast via the hop from benzene to TCNE. In practice, however, the electron of the CT state will be on the TCNE molecule and hence can only hop to another TCNE or benzene molecule, for which the rates are much lower.

In Figures 4.5a and b we see the singlet generation rates, note that they are in general not energy limited (except for the formation due to an electron hop from TCNE to benzene). We see the

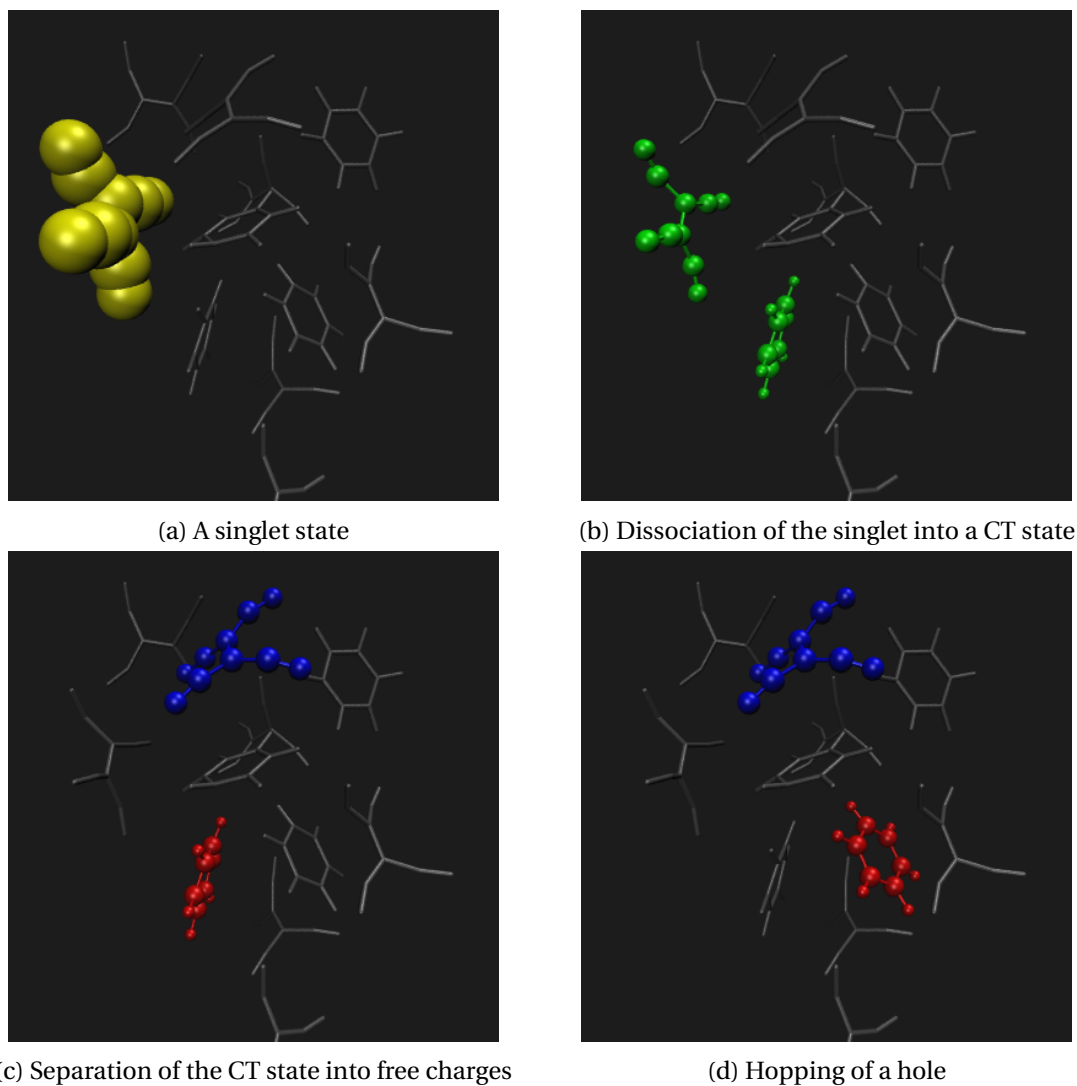


Figure 4.3: A visual summary of the dissociation of a singlet in the simulation. We see a small part of the simulation box in which (a) a singlet state (yellow) is present, that dissociates into a charge transfer state (b) and then separates into free charge (c) that can hop around (d). The blue color is used for negative charges and the red color for positive.

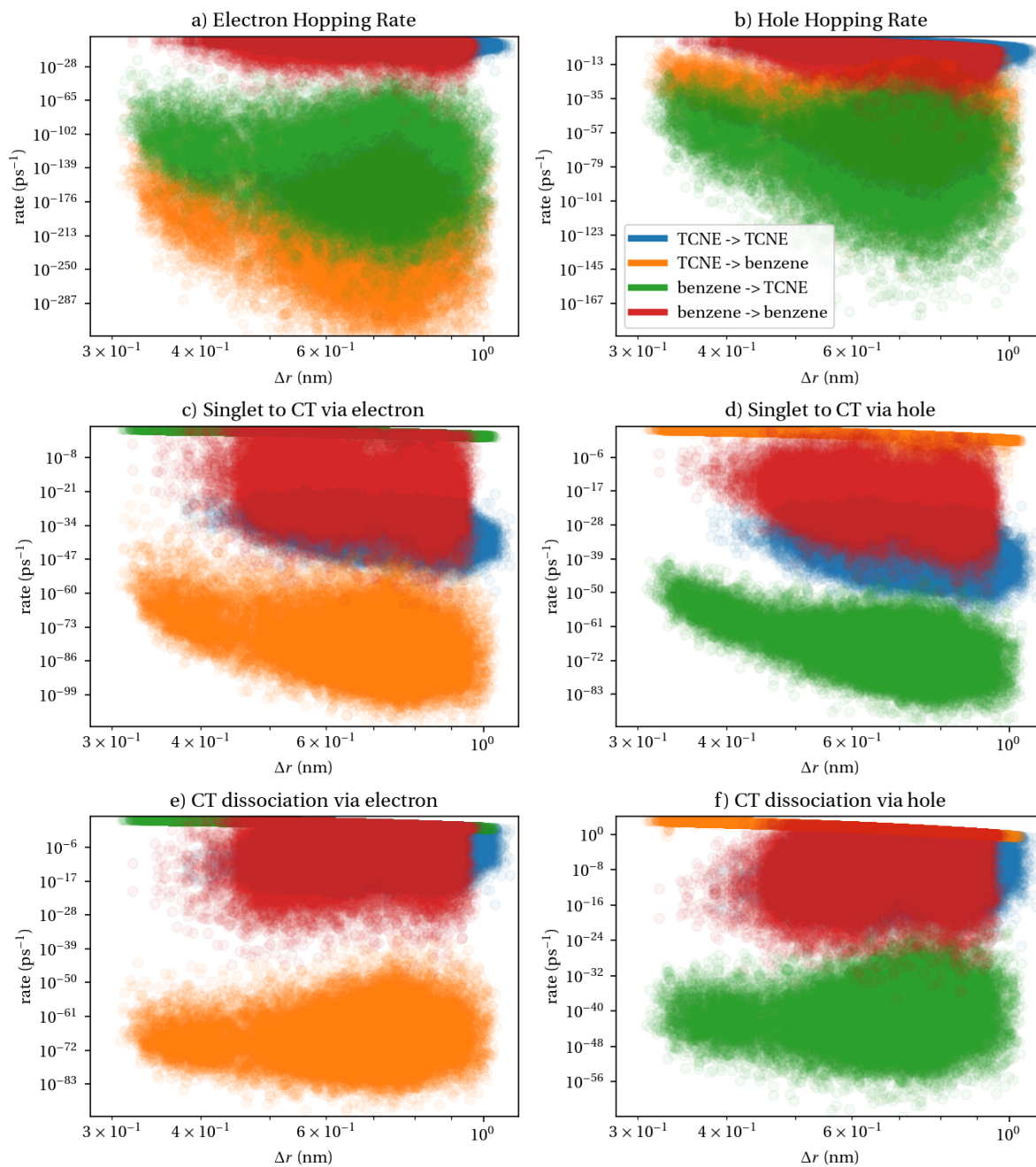


Figure 4.4: The magnitudes of the rates in the KMC model as a function of distance for different processes in the simulation.

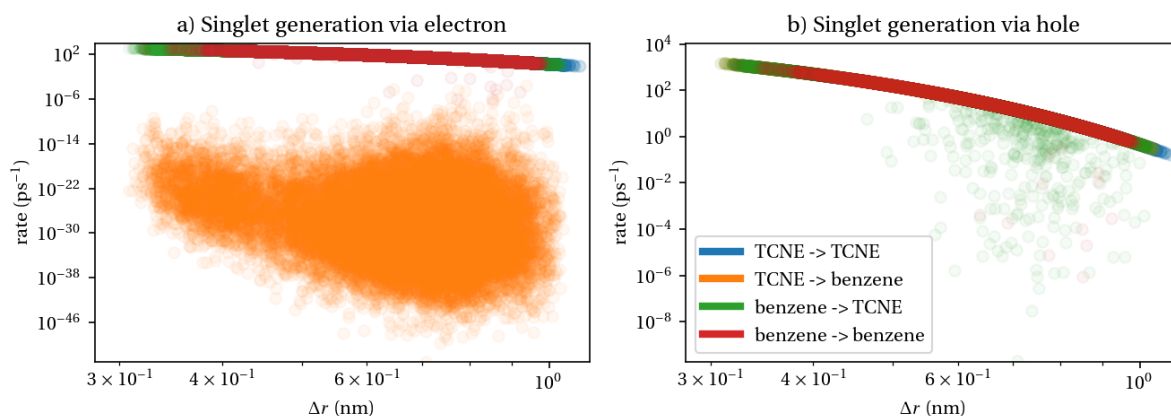


Figure 4.5: The magnitudes of the singlet generation rates as a function of distance.

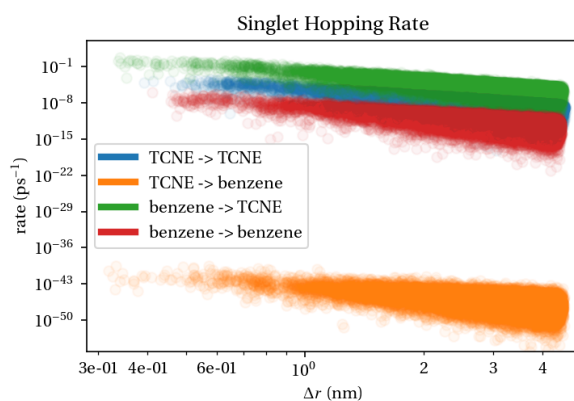


Figure 4.6: Singlet hopping rates for the different possible hops between TCNE and benzene. The hop from TCNE to benzene is orders of magnitudes smaller than the other hopping rates. This is due to the large energy barrier from TCNE to benzene.

exponential decay due to distance and only a very limited amount of energy limited rates. This is explained by the fact that the exciton binding energy is relatively large compared to the site energy differences. This is also expected from literature where it is often assumed that the formation of an exciton (singlet) is always a process downwards in energy [9, 69].

In Figure 4.6 we present the rates for singlet hopping. Note that these rates are at least two orders of magnitude smaller than the hopping rates of electrons and holes. Furthermore we see a splitting in the rates due to hops between different types of molecules. This is not unexpected since the singlet energy differences are large between the two types of molecules. This is also the reason why the rates for hopping from TCNE to benzene are so small.

The rate for singlet decay is on average  $1.7 \cdot 10^{-3} \text{ps}^{-1}$  for a singlet on benzene and  $0.38 \cdot 10^{-3} \text{ps}^{-1}$  for a singlet on TCNE. In the simulation these rates are calculated using the site energies for singlets, here we used the average site energy for the two separate molecules.

#### 4.1.5 Accuracy, Performance and Sensitivity of the Methods

The Monte Carlo method used to simulate the carrier dynamics is statistical in nature. Hence the accuracy of the method heavily depends on the number of simulated events. For Monte Carlo methods, in general, two methods are used to obtain increased accuracy, either simulate more different

trajectories through the state space or simulate longer trajectories. The latter is impossible for the simulation of transient phenomena where the time dependence makes longer simulation useless. Hence in this thesis the first approach is used. Multiple different trajectories were simulated and the results are averaged to obtain the results that we present in the next sections. It was found that 25 trajectories is enough to find reasonably accurate results, the addition of more trajectories to the average did not significantly improve the results obtained.

An advantage of the multiple trajectories to get a higher accuracy is that simulations can be very easily parallelized. A single 1500ps run for the system of 6400 molecules takes just under an hour in most cases. On a computer or server with a high core count this means that even simulating 25 or 50 runs takes one or two hours at most. The KMC simulation also scales very well, linear in the number of carriers present. It is however important to realize that due to the larger cut off of singlets, more possible next events need to be considered for singlets than for electrons or holes, this slows down the simulation considerably. It should also be noted that the KMC scales rather well and is relatively quick, but the parametrization calculations take very long. Parametrization calculations are the main bottleneck for the computational performance. The computation of the coupling elements used in the Marcus rates, for example, can take days to perform even for the small system of 6400 molecules that we consider here. This limits the possibility of simulating multiple different morphologies.

Since most parameters are obtained from *ab initio* calculations the model is almost free of fitting and matching parameters. For that reason the outcomes of the model do not depend heavily on the input parameters. They do, however, depend heavily on the accuracy of the *ab initio* calculations. As we have seen in Section 4.1.4 in particular the energy levels have a large influence on the model. Small differences in the energy levels can result in dramatic changes in the rates of multiple orders of magnitude.

## 4.2 Simulating the Transient Absorption Spectrum

In the previous section we explored the model system and its properties. In this section we present the transient absorption spectrum obtained from the simulation for the model system. We first discuss the carrier dynamics and then the TAS signal.

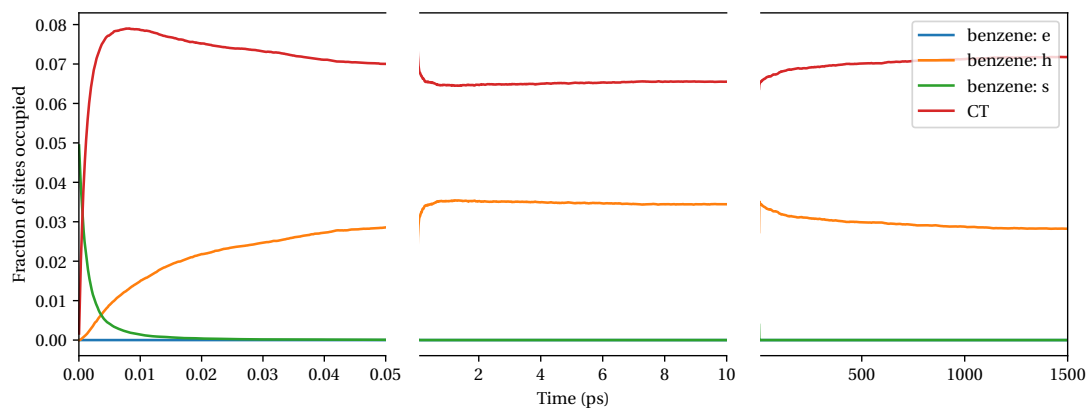
### 4.2.1 Carrier Dynamics

In Figure 4.7a and b we see the carrier dynamics of the system. After the pump pulse 10% of the molecules in the system are excited. As we can see the excited states dissociate very quickly into charge transfer states. Within 0.01ps most excited states have dissociated and many CT states have formed. While the CT states form they already start to dissociate into free charges (e.g. the orange line in Figure 4.7a). Since the CT binding energy is relatively high we see that after the formation of the free charges, the system converges to a situation with many CT states.

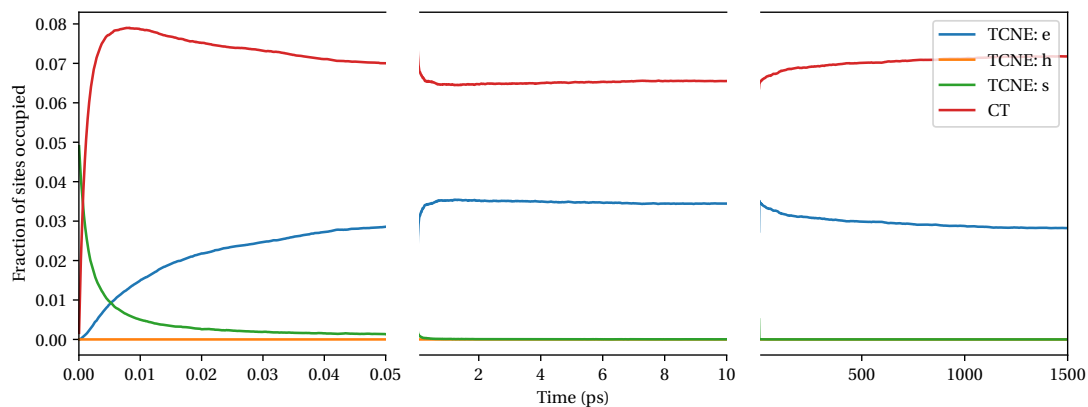
### 4.2.2 Transient Absorption Spectrum

In Figure 4.7c we see the corresponding absorption spectrum. Our main question to answer is if we can couple this spectrum to the carrier dynamics. Starting from the TAS signal at 0.005fs we can clearly see the ground state bleaching (i.e. the negative peaks at t:n and b:n). It is interesting to see that the ground state bleaching increases in the next step forward in time, at 5fs. This is explained by the formation of the large number of CT states that occupy two sites, hence there is approximately twice the amount of sites that are no longer in the ground state. In the time steps that follow we can clearly see the formation of the free charges in the system by the peaks at t:e and b:h. It may be worth noting that due to the donor-acceptor behaviour of the system almost all holes live in benzene sites and all electrons on TCNE sites, this is also clearly visible in the carrier dynamics and TAS signal.

Besides what we do see in the TAS signal it also worth noting what we do not see. First of all we see almost no excited state absorption (ESA) in the TAS signal, this is due to the fact that the absorption of the singlets is weak and the fact that the singlets dissociate so quickly into CT states. This results in a very small number of excited states with a very small absorption and hence they are not visible. We also do not see any stimulated emission, this is expected since it is not accounted for in the model.



(a) Carrier dynamics on the benzene molecules



(b) Carrier dynamics on the TCNE molecules.

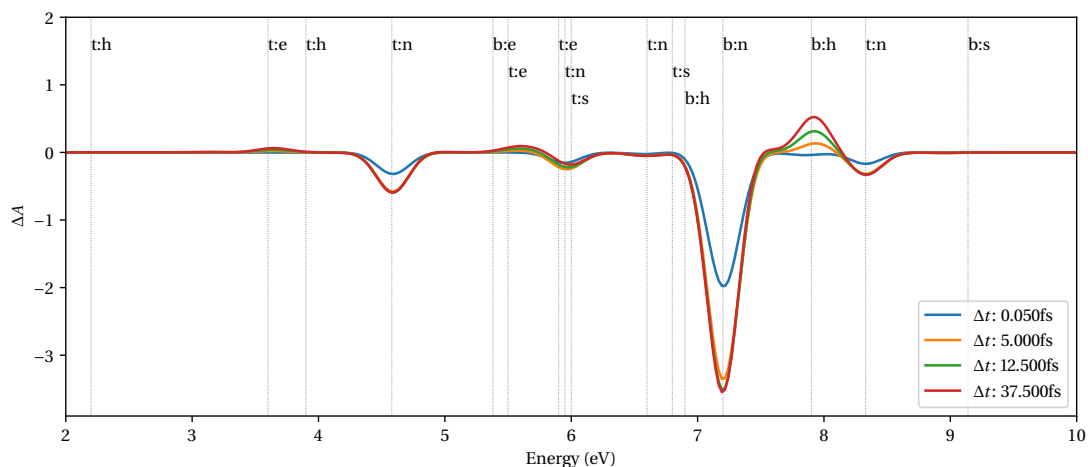
(c) The ( $\Delta A$ ) transient absorption spectrum for different  $\Delta t$ . The vertical dotted lines are visual aids that indicate to which carrier on which molecule a peak belongs, e.g. b:h is a hole on a benzene molecule.

Figure 4.7: The carrier dynamics and transient absorption spectrum of the benzene TCNE mixture.

## 4.3 Simulating Different Cases

Our main goal is to link carrier dynamics to TAS spectra. A single system only leads to one type of dynamic, to investigate different types of dynamics we can either simulate different systems or change parts of the current system. In this section we adopt the latter approach to save on the computational cost associated with the computation of all parameters for different systems. This leads to some interesting, although sometimes unphysical, special cases of the simulation. We consider in order, what would happen if we reduced the CT binding energy, what happens if the energy gaps of the donor-acceptor system are reduced and the case where all molecules get excited by the pump pulse of the transient absorption experiment.

### 4.3.1 Reduced Charge Transfer State Binding Energy

In Figure 4.8 we present what happens if the CT state binding energy is reduced. In the original simulation we saw that the CT binding energy resulted in a large number of CT states at the end of the simulation. If we look at Figures 4.8a and b we still see this effect but it is smaller, there are still quite a lot of CT states, but the number of free charges is now greater than the number of CT states. Also the dynamics just after the pump pulse have changed considerably with the weaker CT binding energy free charges can form easier.

Similar conclusions can be drawn from the TAS signal. We see the same ground state bleach as in the original system and the extra ground state bleach due to the CT states, but what we also see is the increased absorption at the hole peaks of benzene and electron peaks of TCNE. This is in line with the increased number of free charges observed in the carrier dynamics.

### 4.3.2 Reduced Gap Between Donor and Acceptor

The main feature of the model system is its extreme donor-acceptor behaviour. In Figure 4.9 we present what happens if we make this effect less pronounced. We reduced the HOMO gap between the two molecules by 1.0 eV, the LUMO gap between the molecules by 2.5 eV and the singlet gap by 2.2 eV. The new DOS is presented in Figure 4.10.

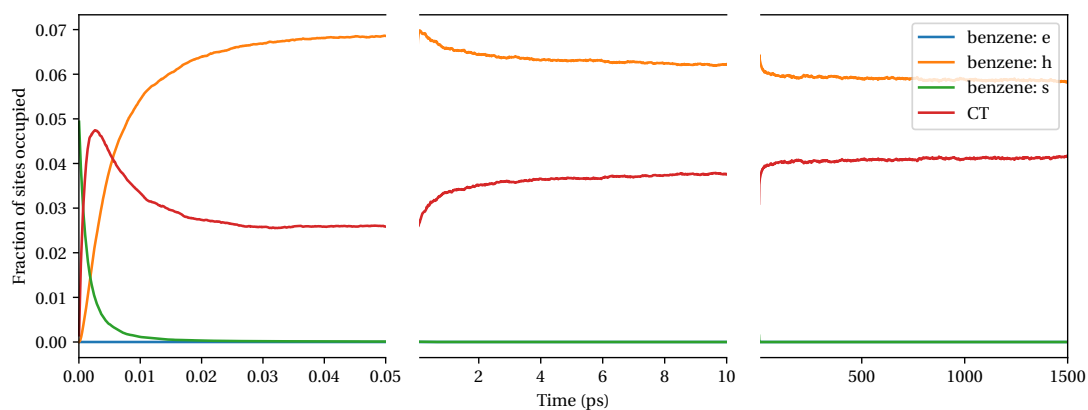
In Figure 4.9a and b we see the effect on the carrier dynamics of this change in energy gaps. At first glance it does not appear much different from the original system, but nonetheless there is some difference. We see that the singlets are less easily split into CT states and more singlets remain over a longer period of time (see the green lines in both graphs). This is exactly what one expects from a system with a smaller acceptor-donor gap. For the same reason we also see that it takes longer for the free charges to appear in large numbers.

In the TAS signal we see the same as in the original case and the fact that the electrons and holes take longer to form (the absorption peaks are smaller).

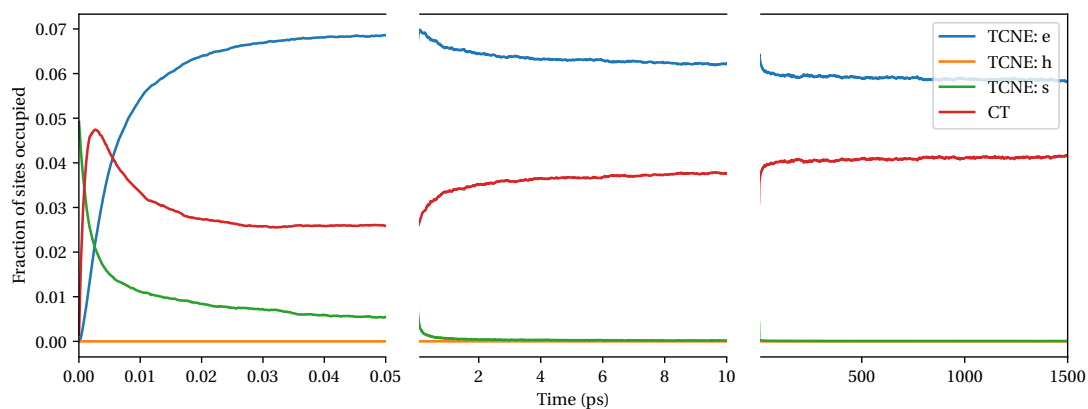
### 4.3.3 All Singlets

Physically very unlikely, but interesting as a limiting case, we consider what would happen if the pump pulse of the TAS experiment would excite every single molecule in the system, i.e. after the pump pulse every site is in the singlet state. The results of this numerical experiment are presented in Figure 4.11.

In Figures 4.11a and b we see how the carrier dynamics have changed, instead of the very fast processes that we saw before, we see a very slow decay of singlets and a slow rise of CT states for both the benzene and TCNE molecule. This can be explained as follows; if every site is in the singlet state it is impossible for a singlet to dissociate into a CT state, instead we need to wait for singlets to



(a) Carrier dynamics on the benzene molecules



(b) Carrier dynamics on the TCNE molecules.

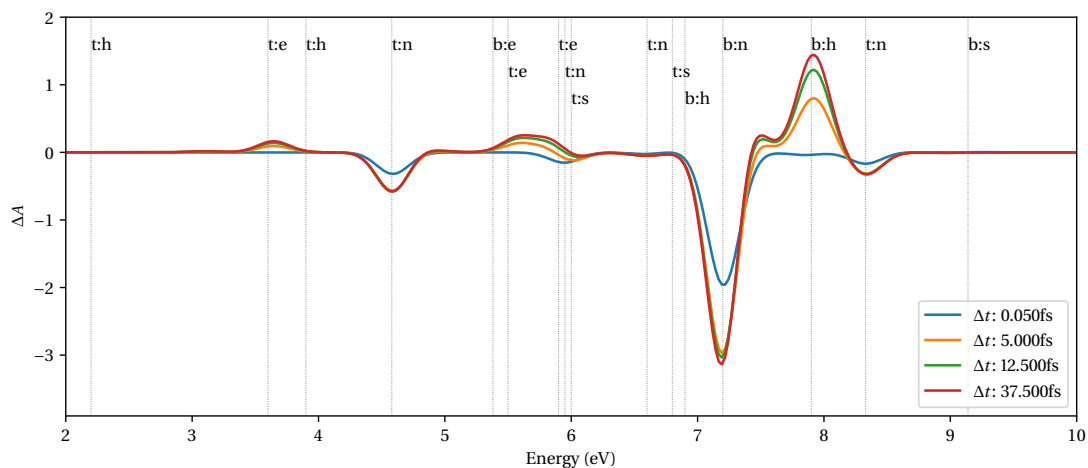
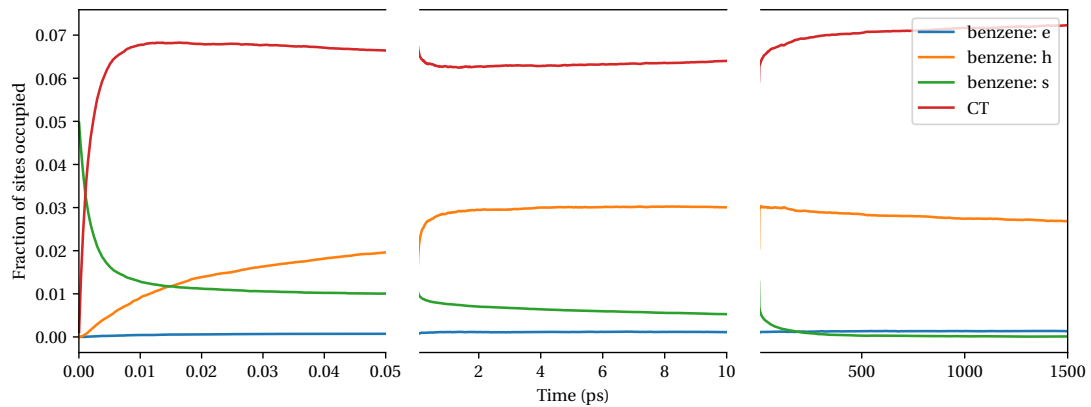
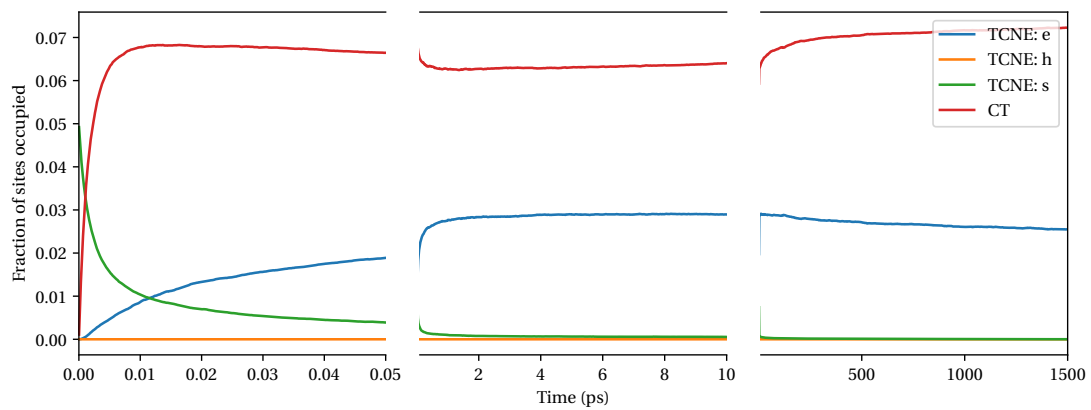
(c) The ( $\Delta A$ ) transient absorption spectrum for different  $\Delta t$ . The vertical dotted lines are visual aids that indicate to which carrier on which molecule a peak belongs, e.g. b:h is a hole on a benzene molecule.

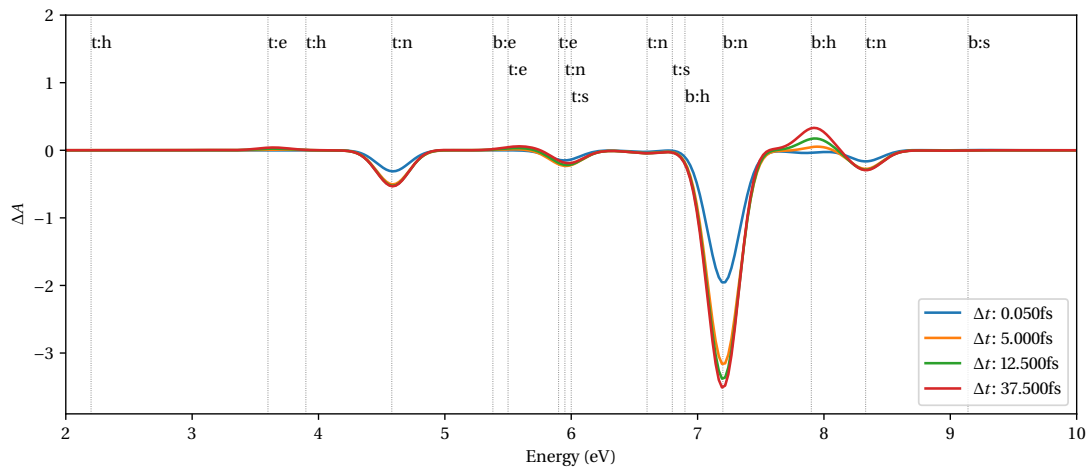
Figure 4.8: The carrier dynamics and transient absorption spectrum of the benzene TCNE mixture, where the CT binding energy has been reduced by a factor of four.



(a) Carrier dynamics on the benzene molecules



(b) Carrier dynamics on the TCNE molecules.



(c) The ( $\Delta A$ ) transient absorption spectrum for different  $\Delta t$ . The vertical dotted lines are visual aids that indicate to which carrier on which molecule a peak belongs, e.g. b:h is a hole on a benzene molecule.

Figure 4.9: The carrier dynamics and transient absorption spectrum of the benzene TCNE mixture, with a reduced difference in energy between the donor and acceptor, the corresponding DOS is presented in Figure 4.10.

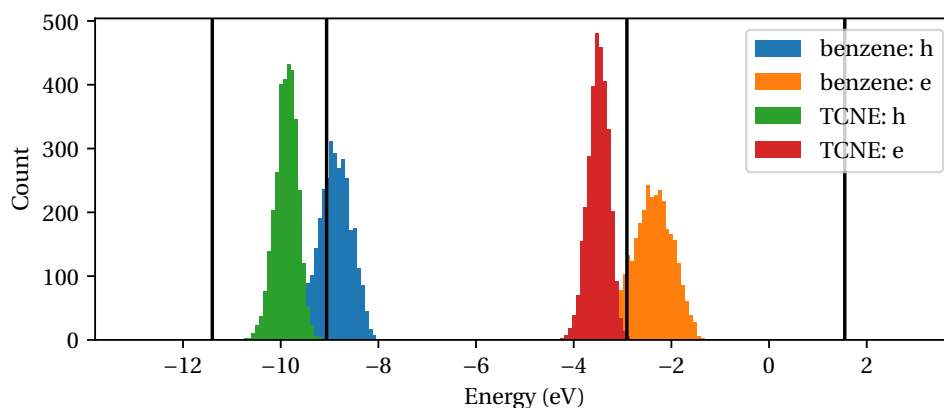
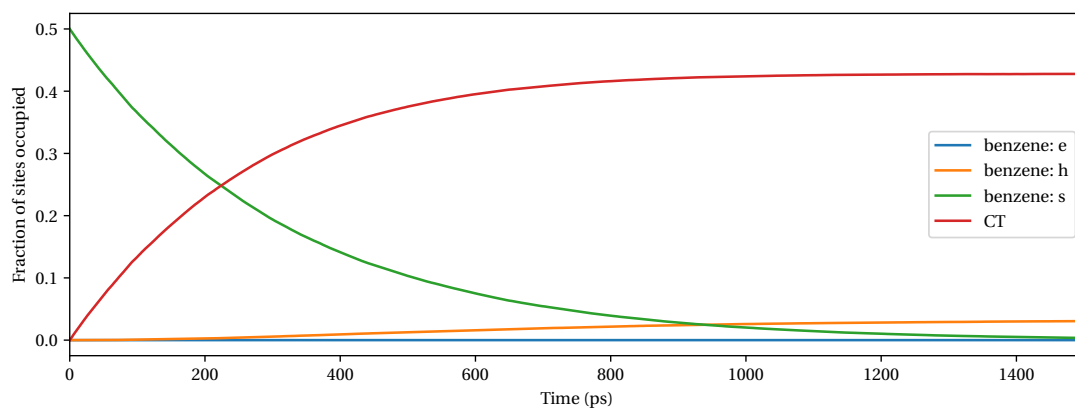


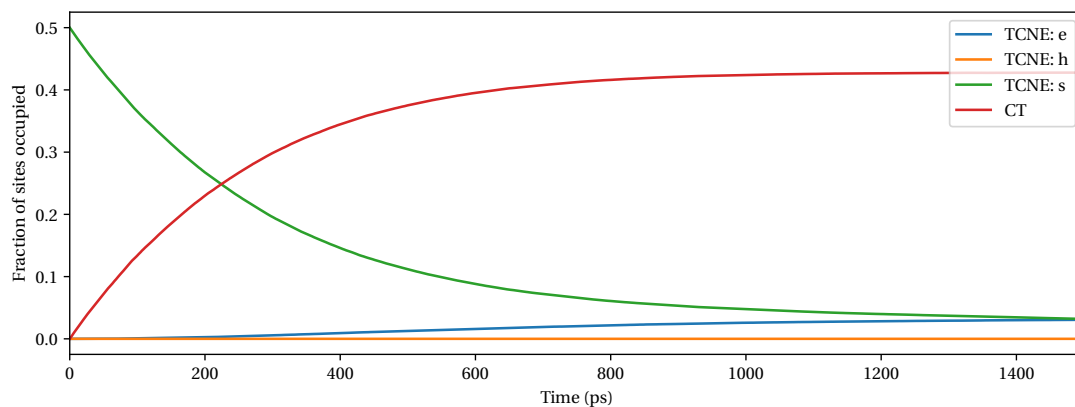
Figure 4.10: The DOS corresponding to the results presented in Figure 4.9. The TCNE HOMO level has been heightened by 1.0 eV and the benzene LUMO has been lowered by 2.5 eV. The singlet level of benzene (although not displayed) has also been lowered by 2.2 eV to reduce the singlet gap as well.

decay. As we have seen in Section 4.1.4, the exciton decay process is much slower than the dissociation processes. Once a singlet has decayed another singlet in proximity to the decayed singlet will dissociate into a CT state (very fast process) once again blocking all other processes from occurring and we need to wait again for a singlet to decay before something else can happen. This repeats itself for quite some time after which enough singlets have decayed to also allow for the formation of free charges.

In Figure 4.11c we see the corresponding TAS signal for different time steps. Since all sites are in the singlet state after the pump pulse, the ground state bleach is quite extreme, there is no molecule that is not excited. Due to the almost instantaneous formation of CT states after exciton decay, the ground state bleach also does not really decrease in time, and hence this process can not or hardly be deduced from the TAS signal. The only process we can truly observe in the TAS signal is the formation of the free charges.



(a) Carrier dynamics on the benzene molecules



(b) Carrier dynamics on the TCNE molecules.

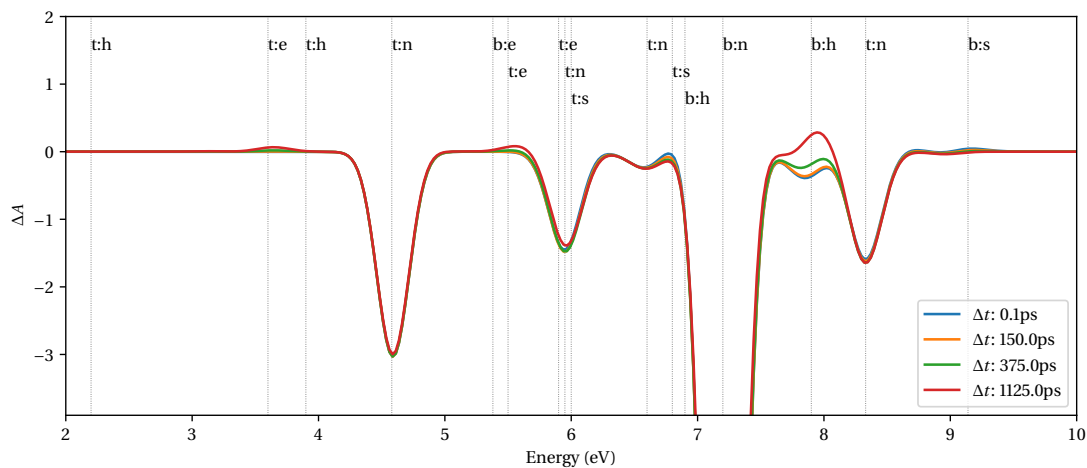
(c) The ( $\Delta A$ ) transient absorption spectrum for different  $\Delta t$ . The vertical dotted lines are visual aids that indicate to which carrier on which molecule a peak belongs, e.g. b:h is a hole on a benzene molecule.

Figure 4.11: The carrier dynamics and transient absorption spectrum of the benzene TCNE mixture, where all molecules are excited at the start.

# Chapter 5

## Conclusion and Future Work

### 5.1 Conclusions

The results of this thesis show that ab initio methods can be advantageously combined with a statistical model to model transient absorption spectra of disordered molecular systems. We have seen that spectral features of the simulated TAS signal can be linked to the underlying processes within the simulation. In particular we saw that charge transfer states may contribute heavily to the ground state bleaching in the spectrum. By varying different parameters in the model we have seen that carrier dynamics are very sensitive to the relative energy levels of the molecules. Also the charge transfer state binding energy determines to a large extent to what equilibrium the dynamics will converge. In conclusion we can answer our starting question from Section 1.4 with an affirmative answer, it is possible to develop a model that can assist in inferring dynamical processes from transient absorption spectra. Indeed, the presented model helps and proves the concept. For it to be used to predict experimental outcomes, however, improvements need to be made that we discuss in the next section.

### 5.2 Future Work

#### 5.2.1 Improving the Model

The multiscale model presented in this thesis is a first step towards a full model for transient absorption in organic materials. However, different parts of the model can be improved upon, we list the most important possible improvements:

- Currently only the charge and exciton transfer models are modelled via the Marcus rate. For the processes involving the generation or dissociation of species we had to fall back on the Miller-Abraham's formalism in which the parameters were obtained through a fitting procedure. This will only give approximate results. A more formal and accurate rate to predict the dissociation and generation of species is necessary.
- An important interaction between the carriers in an organic material is the Coulomb interaction. In the current model it is ignored except in the case of CT-states. In a future version of the model the Coulomb interaction should be included to allow for more realistic dynamics. A starting point for an efficient Coulomb interaction implementation could be the recent paper by Pippig and Mercuri [53].
- The only pathway for carriers to decay in the simulation is through singlet decay. It is however known that more pathways exist. For example holes and electrons can meet and annihilate one another instead of forming an exciton, also excitons can meet and destroy one another. These extra pathways could be included in future versions of the KMC simulation.

- The coupling between the output of the KMC model and the absorption spectra is based on the spectra of the different species in vacuum. To simulate the effect of interaction between the molecules and electron-vibration coupling, the spectra are broadened via a convolution with a Gaussian or Lorentzian kernel. It is however also possible to compute the absorption spectra for every site including the interaction with neighbours and electron-vibration coupling [70]. This would allow the simulation of more detailed absorption spectra. In particular it would be possible to see to what extent carriers move to sites of lower energy in the time of a transient absorption experiment.
- In the simulated transient absorption spectrum we only account for ground state bleach and excited state absorption. It would be beneficial to also include stimulated emission.
- The current KMC implementation is not optimized although some optimizations are possible. First of all, some processes have rates that are so small that their probability of occurring is almost zero, they could be ignored, this would save memory and computation time, since the number of possible next events would become much smaller. The difficulty in this optimization is that the timescales of processes can change drastically with changing parameters and hence which events can be ignored is very parameter and system dependent. Another possible optimization is to check for bimolecular trap states, these are states where the rates between two neighbouring sites are very high to jump from one to another. Carriers, hopping between these two sites, do not contribute much to the overall dynamics and make the simulation much slower. It should be investigated if these states can be eliminated or circumvented.

### 5.2.2 Different Approaches to Carrier Dynamics

Besides improving this model, completely different approaches to carrier dynamics could be considered as well.

#### Focussing on the very small

The master equation approach already considers the carrier hopping as random walks on a graph. The random walk approach could however be extended. There are branching and annihilating random walk processes that could potentially be adapted to obtain information about exciton behaviour such as lifetimes, distances travelled and time until dissociation or in the case of annihilating random walks the time until a positive and negative charge meet and form an exciton. Another random model, the parabolic Anderson model, provides a way to investigate random walks in a random potential (e.g. the disordered energy landscape of an organic material) [71]. Also work has been done on the study of multiple random walks and interacting particle systems [72] that looks at information exchange between meeting particles on a graph, which shows similarities to the formation of an exciton.

While random walk methods will most likely never replace the flexibility and versatility of the kinetic Monte Carlo approach, they may be able to provide theoretical insight and could be used to verify the correct implementation of specific processes in KMC models.

#### Focussing on the very large

Considering the results of the carrier dynamics such as Figure 4.7 and 4.8, the results look like that of a compartment model. A compartment model is a model where different species (electrons, holes, CT states etc.) can turn into one another at certain rates. A good example is the SIR model for infectious disease modelling. This similarity between the results and a compartment model may

indicate that there are continuous differential equations that can approximate the behaviour of the dissociation of singlets into CT states and into free charges and the other way around. This would give an approach to carrier dynamics that can very quickly and easily model transient absorption spectra at least approximately.

# Appendix A

## Computation of Transition Dipoles

Transition dipoles are computed from wave functions, representing states. Suppose we have two states, represented by the wave functions  $\psi_1$  and  $\psi_2$  then the transition dipole between these two states is  $\langle \psi_1 | \hat{d} | \psi_2 \rangle$ . Here we will compute two kinds of transition dipoles, transition dipoles from the ground state to the  $i$ th excited state (i.e.  $\langle 0 | \hat{d} | S_i \rangle$ ) and transition dipoles between excited states (i.e.  $\langle S_i | \hat{d} | S_j \rangle$ ). We will first discuss the representation of the states and then perform the computations.

### A.1 Representation of the Ground State

The starting point for our representations are atomic orbitals (AOs),  $\chi_\mu$ . Using a self-consistent field (SCF) approach like density functional theory (DFT), we can obtain the molecular orbitals (MOs),  $\phi_i$ , as linear combinations of AOs,

$$\phi_i = \sum_{\mu} c_{\mu i} \chi_{\mu}. \quad (\text{A.1})$$

Every MO can be occupied by two electrons with opposite spin. We use  $\phi_i$  for the wave function of the spin up electron and  $\bar{\phi}_i$  for the spin down. Using these spin orbitals we can represent the ground state of a closed shell system with  $n$  electrons by a Slater determinant

$$|\emptyset\rangle = \psi_0 = |\phi_1(1)\bar{\phi}_1(2) \dots \phi_{n/2}(n-1)\bar{\phi}_{n/2}(n)| = \begin{vmatrix} \phi_1(1) & \phi_1(2) & \phi_1(3) & \dots \\ \bar{\phi}_1(1) & \bar{\phi}_1(2) & \bar{\phi}_1(3) & \dots \\ \phi_2(1) & \phi_2(2) & \phi_2(3) & \dots \\ \vdots & \vdots & \vdots & \ddots \end{vmatrix}. \quad (\text{A.2})$$

### A.2 Representation of the Excited State

The following discussion is based on the first chapter of [73] in which excited states are represented as linear combinations of singly excited states.

#### A.2.1 Singly Excited States

A singly excited state is a state where exactly one electron is moved from the ground state to a higher unoccupied state. We will use the notation  $\psi_{i \rightarrow k}$  to indicate such a state, where the electron previously in orbital  $i$ , is now in orbital  $k$ . Note that we do not specify which electron has moved from orbital  $i$  it could be the spin up or spin down electron. This implies that our singly excited state is a linear combination of two states namely

$$\psi_{i \rightarrow k} = \frac{1}{\sqrt{2}} (|\phi_1\bar{\phi}_1 \dots \phi_i\bar{\phi}_k \dots \phi_{n/2}\bar{\phi}_{n/2}| + |\phi_1\bar{\phi}_1 \dots \phi_k\bar{\phi}_i \dots \phi_{n/2}\bar{\phi}_{n/2}|). \quad (\text{A.3})$$

### A.2.2 Excited States (TDA)

An excited state can now be expressed (approximated) as a linear combination of singly excited states

$$|S_i\rangle = \sum_K C_K^i \psi_K, \quad K \in \{0 \rightarrow 1, \dots, i \rightarrow k\}. \quad (\text{A.4})$$

In principle we should also include doubly, triply etc. excited states in the linear combination, however their occurrence is rare and can therefore be safely ignored in most cases. Equation A.4 is known as the Tamm-Dancoff approximation where we only allow for electron-hole pair creation. In literature equation A.4 is also represented as

$$|S_i\rangle = \sum_v^{\text{occ}} \sum_c^{\text{empty}} A_{vc}^i \psi_{v \rightarrow c}. \quad (\text{A.5})$$

### A.2.3 Excited States (RPA)

A more advanced approximation of the excited states is obtained if we not only include singly excited states but also allow for singly de-excited states

$$|S_i\rangle = \sum_v^{\text{occ}} \sum_c^{\text{empty}} [A_{vc}^i \psi_{v \rightarrow c} + B_{vc}^i \psi_{c \rightarrow v}]. \quad (\text{A.6})$$

## A.3 Transition dipoles between the ground and excited states

### Within the TDA

$$\begin{aligned} \langle S_i | \hat{d} | \emptyset \rangle &= \left\langle \sum_v^{\text{occ}} \sum_c^{\text{empty}} A_{vc}^i \psi_{v \rightarrow c} \middle| \hat{d} \middle| \emptyset \right\rangle \\ &= \sum_{vc} \langle A_{vc}^i \psi_{v \rightarrow c} | \hat{d} | \emptyset \rangle \\ &= \sum_{vc} A_{vc}^i \langle \psi_{v \rightarrow c} | \hat{d} | \emptyset \rangle \end{aligned} \quad (\text{A.7})$$

Now we apply ‘‘Slater’s rules’’ for the computation of matrix elements between Slater determinants (see section A.5). Note that the dipole operator is a sum of one particle operators and hence we only need to consider the one particle operator part of Slater’s rules.

$$\begin{aligned} \langle \psi_{v \rightarrow c} | \hat{d} | \emptyset \rangle &= \frac{1}{\sqrt{2}} \left( \langle \phi_c | \hat{d} | \phi_v \rangle + \langle \bar{\phi}_c | \hat{d} | \bar{\phi}_v \rangle \right) \\ &= \sqrt{2} \langle \phi_c | \hat{d} | \phi_v \rangle \end{aligned} \quad (\text{A.8})$$

In the last line we used that fact that we only know that one of the two electrons is excited from the  $v$  orbital, we don’t know which one. Nonetheless the effect should be the same. Finally the transition dipole is

$$\langle S_i | \hat{d} | \emptyset \rangle = \sqrt{2} \sum_{vc} A_{vc}^i \langle \phi_c | \hat{d} | \phi_v \rangle. \quad (\text{A.9})$$

### Within the RPA

Extension of the previous procedure to the RPA case is easy now

$$\begin{aligned}
\langle S_i | \hat{d} | \emptyset \rangle &= \left\langle \sum_v^{occ} \sum_c^{empty} [A_{vc}^i \psi_{v \rightarrow c} + B_{vc}^i \psi_{c \rightarrow v}] | \hat{d} | \emptyset \right\rangle \\
&= \sum_{vc} [\langle A_{vc}^i \psi_{v \rightarrow c} | \hat{d} | \emptyset \rangle + \langle B_{vc}^i \psi_{c \rightarrow v} | \hat{d} | \emptyset \rangle] \\
&= \sum_{vc} [A_{vc}^i \langle \psi_{v \rightarrow c} | \hat{d} | \emptyset \rangle + B_{vc}^i \langle \psi_{c \rightarrow v} | \hat{d} | \emptyset \rangle] \\
&= \sum_{vc} \left[ A_{vc}^i \sqrt{2} \langle \phi_c | \hat{d} | \phi_v \rangle + B_{vc}^i \sqrt{2} \langle \phi_v | \hat{d} | \phi_c \rangle \right] \\
&= \sqrt{2} \sum_{vc} (A_{vc}^i + B_{vc}^i) \langle \phi_c | \hat{d} | \phi_v \rangle.
\end{aligned} \tag{A.10}$$

Here we used that  $\langle \phi_c | \hat{d} | \phi_v \rangle = \langle \phi_v | \hat{d} | \phi_c \rangle$ .

## A.4 Transition dipoles between excited states

### A.4.1 Representation of the Electron-Hole Pair

To represent the electron-hole pair we switch to a product basis of single particle electron and hole wavefunctions. Assuming that a state in this product basis is a linear combination of Slater determinants we get

$$\begin{aligned}
|S_i\rangle &= \sum_v^{occ} \sum_c^{empty} [A_{vc}^i |\phi_v \phi_c\rangle + B_{vc}^i |\phi_c \phi_v\rangle] \\
&= \sum_{vc} (A_{vc}^i - B_{vc}^i) |\phi_v \phi_c\rangle \\
&= \sum_{vc} D_{vc}^i |\phi_v \phi_c\rangle.
\end{aligned} \tag{A.11}$$

### A.4.2 Transition dipoles

Transition dipoles between excited states are easily computed from the representation (A.11).

$$\begin{aligned}
\langle S_i | \hat{d} | S_j \rangle &= \left\langle \sum_{vc} D_{vc}^i |\phi_v \phi_c\rangle | \hat{d} | \sum_{v'c'} D_{v'c'}^j |\phi_{v'} \phi_{c'}\rangle \right\rangle \\
&= \sum_{vc} \sum_{v'c'} D_{vc}^i D_{v'c'}^j \langle |\phi_v \phi_c\rangle | \hat{d} | |\phi_{v'} \phi_{c'}\rangle \rangle
\end{aligned} \tag{A.12}$$

Using Slater's rules for matrix elements we can compute the remaining matrix element

$$\langle |\phi_v \phi_c\rangle | \hat{d} | |\phi_{v'} \phi_{c'}\rangle \rangle = \langle \phi_v | \hat{d} | \phi_{v'} \rangle \delta_{cc'} + \langle \phi_c | \hat{d} | \phi_{c'} \rangle \delta_{vv'}. \tag{A.13}$$

Hence we get

$$\langle S_i | \hat{d} | S_j \rangle = \sum_{vc} \sum_{v'c'} D_{vc}^i D_{v'c'}^j \left( \langle \phi_v | \hat{d} | \phi_{v'} \rangle \delta_{cc'} + \langle \phi_c | \hat{d} | \phi_{c'} \rangle \delta_{vv'} \right). \tag{A.14}$$

For the actual implementation of this calculation in the software package VOTCA we can split the summation into a valence part  $V$  and a conduction part  $C$ , due to the Kronecker delta

$$\langle S_i | \hat{d} | S_j \rangle = V + C \quad (\text{A.15})$$

$$V = \sum_{vv'} \sum_c D_{vc}^i D_{v'c}^j \langle \phi_v | \hat{d} | \phi_{v'} \rangle \quad (\text{A.16})$$

$$C = \sum_{cc'} \sum_v D_{vc}^i D_{v'c'}^j \langle \phi_c | \hat{d} | \phi_{c'} \rangle. \quad (\text{A.17})$$

The coefficients  $E_{vv'} = \sum_c D_{vc}^i D_{v'c}^j$  and  $F_{cc'} = \sum_v D_{vc}^i D_{v'c'}^j$  are obtained via matrix multiplication,  $E = D^i \cdot (D^j)^T$  and  $F = (D^i)^T \cdot D^j$ . We are left with

$$V = \sum_{vv'} E_{vv'} \langle \phi_v | \hat{d} | \phi_{v'} \rangle \quad (\text{A.18})$$

$$C = \sum_{cc'} F_{cc'} \langle \phi_c | \hat{d} | \phi_{c'} \rangle \quad (\text{A.19})$$

$$\langle S_i | \hat{d} | S_j \rangle = V + C. \quad (\text{A.20})$$

## A.5 Slater's Rules for Matrix Elements

We present Slater's rules for the one particle operator  $h$  and two particle operator  $g$ , based on [74]. We start from the operator  $H = h + g$  acting on a state  $\Phi$  which is a product of spin-orbitals  $\psi_i$  and assume that all spin-orbitals are orthonormal.

The diagonal element equals

$$\langle \Phi | H | \Phi \rangle = \sum_R \langle \psi_R | h | \psi_R \rangle + \frac{1}{2} \sum_{R,S} (\langle \psi_R \psi_S | g | \psi_R \psi_S \rangle - \langle \psi_R \psi_S | g | \psi_S \psi_R \rangle). \quad (\text{A.21a})$$

Matrix elements with one spin-orbital difference ( $\psi_R \neq \psi'_R$ ) equal

$$\langle \Phi' | H | \Phi \rangle = \langle \psi'_R | h | \psi_R \rangle + \sum_{R \neq S} (\langle \psi'_R \psi_S | g | \psi_R \psi_S \rangle - \langle \psi'_R \psi_S | g | \psi_S \psi_R \rangle). \quad (\text{A.21b})$$

Matrix elements with two spin-orbital differences ( $\psi_R \neq \psi'_R$  and  $\psi_S \neq \psi'_S$ ) are equal to

$$\langle \Phi' | H | \Phi \rangle = \langle \psi'_R \psi'_S | g | \psi_R \psi_S \rangle - \langle \psi'_R \psi'_S | g | \psi_S \psi_R \rangle. \quad (\text{A.21c})$$

# Appendix B

## The Master Equation Extras

### B.1 Solving the Pauli Master Equation

In Chapter 3 the master equation was discussed here we briefly present three ways of solving the Pauli Master Equation. Firstly there is the popular iterative method by Yu et al. [75]. This boils down to sequentially updating the average site occupations according to

$$f_i = 1 / \left[ 1 + \frac{\sum_j v_{i \rightarrow j} (1 - f_j)}{\sum_j v_{j \rightarrow i} f_j} \right], \quad (\text{B.1})$$

until satisfactory convergence has been reached. Note that as soon as a value is updated it will be used for all further calculations (this is called implicit calculation in the Yu et al. paper).

A second method is based on Newton's method, smart ways of computing the Jacobian have been developed to solve the system [76]. According to [76] the most efficient way of solving the system of equations however is a combined approach in which Newton's method is used predominately and an occasional "correction" step is performed via Yu's method.

When using the Newton method, Equation 3.13 ( $\sum_i f_i = N$ ) can be "spread" over the Pauli Master Equation as follows,

$$g_i(\vec{f}) = \left[ \sum_{j \neq i} v_{j \rightarrow i} f_j (1 - f_i) - v_{i \rightarrow j} f_i (1 - f_j) \right] + \frac{t_c v_0 p_i (1 - p_i)}{\sqrt{\sum_i f_i^2 (1 - f_i)^2}} \left[ N - \sum_i f_i \right] = 0, \quad (\text{B.2})$$

where the factor  $v_0 p_i (1 - p_i)$  is added to make sure that both terms are of a comparable size and  $t_c$  is the concentration tuning factor (an indicator for how much relative error we allow in the carrier concentration)[76].

### B.2 The Master Equation for Multiple Particles of Different Types

Equation 3.12 can be further extended to include generation and recombination of electrons and holes [77]. The approach is to consider separate site occupations for electrons and holes,  $p_{i,e}$  and  $p_{i,h}$  respectively. If a site is occupied by both a hole and an electron there is a rate for recombination  $1/\tau$  and if a site is empty (no holes or electrons) generation of an electron hole pair can occur with a generation rate of  $c_i/\tau$ . The new master equations are

$$\frac{dp_{i,e}}{dt} = \sum_{j \neq i} \left[ -p_{i,e} v_{ij,e} (1 - p_{j,e}) + p_{j,e} v_{ji,e} (1 - p_{i,e}) \right] - \frac{p_{i,e} p_{i,h}}{\tau} + c_i \frac{(1 - p_{i,e})(1 - p_{i,h})}{\tau}, \quad (\text{B.3})$$

$$\frac{dp_{i,h}}{dt} = \sum_{j \neq i} \left[ -p_{i,h} v_{ij,h} (1 - p_{j,h}) + p_{j,h} v_{ji,h} (1 - p_{i,h}) \right] - \frac{p_{i,e} p_{i,h}}{\tau} + c_i \frac{(1 - p_{i,e})(1 - p_{i,h})}{\tau}. \quad (\text{B.4})$$

The generation/recombination process must satisfy the principle of detailed balance at equilibrium and, with the assumption of Fermi-Dirac statistics, the coefficient  $c_i$  can be calculated as [77]

$$c_i = \frac{p_{i,e}p_{j,h}}{(1-p_{i,e})(1-p_{i,h})} = \exp\left(\frac{E_{i,h} - E_{i,e}}{k_B T}\right). \quad (\text{B.5})$$

# Bibliography

- [1] W. Humphrey, A. Dalke, and K. Schulten, “{VMD} – {V}isual {M}olecular {D}ynamics,” *Journal of Molecular Graphics*, vol. 14, pp. 33–38, 1996.
- [2] “AMOLED set for wireless dominance, with more than half of smartphones using the display technology by 2023 - Omdia,” nov 2019.
- [3] O. A. Abdulrazzaq, V. Saini, S. Bourdo, E. Dervishi, and A. S. Biris, “Organic solar cells: A review of materials, limitations, and possibilities for improvement,” *Particulate Science and Technology*, vol. 31, no. 5, pp. 427–442, 2013.
- [4] V. Coropceanu, J. Cornil, D. A. da Silva Filho, Y. Olivier, R. Silbey, and J. L. Brédas, “Charge transport in organic semiconductors,” *Chemical Reviews*, vol. 107, no. 4, pp. 926–952, 2007.
- [5] Y. Shirota and H. Kageyama, “Charge carrier transporting molecular materials and their applications in devices,” *Chemical Reviews*, vol. 107, no. 4, pp. 953–1010, 2007.
- [6] H. Bässler, “Charge Transport in Disordered Organic Photoconductors a Monte Carlo Simulation Study,” *Physica Status Solidi (B)*, vol. 175, no. 1, pp. 15–56, 1993.
- [7] R. Berera, R. van Grondelle, and J. T. Kennis, “Ultrafast transient absorption spectroscopy: Principles and application to photosynthetic systems,” *Photosynthesis Research*, vol. 101, no. 2-3, pp. 105–118, 2009.
- [8] K. Nishimura, F. S. Rondonuwu, R. Fujii, J. Akahane, Y. Koyama, and T. Kobayashi, “Sequential singlet internal conversion of  $1\text{Bu}^+ \rightarrow 3\text{Ag}^- \rightarrow 1\text{Bu}^- \rightarrow 2\text{A g}^- \rightarrow (1\text{Ag}^- \text{ ground})$  in all-trans-spirilloxanthin revealed by two-dimensional sub-5-fs spectroscopy,” *Chemical Physics Letters*, vol. 392, no. 1-3, pp. 68–73, 2004.
- [9] V. Eersel, *Device physics of organic light-emitting diodes: interplay between charges and excitons*. PhD thesis, TU Eindhoven, 2015.
- [10] M. Born and R. Oppenheimer, “Zur Quantentheorie der Molekeln,” *Annalen der Physik*, vol. 84, 1927.
- [11] J. Kohanoff, “Electronic structure calculations for solids and molecules: Theory and computational methods,” 2006.
- [12] F. Bechstedt, *Many-Body Approach to Electronic Excitations: Concepts and Applications*. Springer, 2014.
- [13] T. Koopmans, “Über die Zuordnung von Wellenfunktionen und Eigenwerten zu den Einzelnen Elektronen Eines Atoms,” *Physica*, vol. 1, no. 1-6, pp. 104–113, 1934.
- [14] C. Roothaan, “New Developments in Molecular Orbital Theory,” *Reviews of Modern Physics*, vol. 23, no. 2, pp. 69–89, 1951.

- [15] T. Tsuneda, *Density Functional Theory in Quantum Chemistry*. Springer Tokyo Heidelberg, 2014.
- [16] F. Jensen, *Introduction to Computational Chemistry Computational Chemistry*. Wiley, 2017.
- [17] C. D. Sherrill and H. F. Schaefer, "The Configuration Interaction Method: Advances in Highly Correlated Approaches," in *Advances in Quantum Chemistry* (P.-O. Löwdin, J. R. Sabin, M. C. Zerner, and E. Brändas, eds.), vol. 34 of *Advances in Quantum Chemistry*, pp. 143–269, Academic Press, 1999.
- [18] J. Čížek, "On the Use of the Cluster Expansion and the Technique of Diagrams in Calculations of Correlation Effects in Atoms and Molecules," jan 1969.
- [19] W. Kohn, "Electronic Structure of Matter - Wave Functions and Density Functionals," 1999.
- [20] P. Hohenberg and W. Kohn, "Inhomogeneous Electron Gas," *Physical Review*, vol. 136, no. 3, pp. 864–870, 1964.
- [21] R. Parr and W. Yang, "Density-Functional Theories of Atoms and Molecules," 1989.
- [22] W. Kohn and J. Sham, "Self-Consistent Equation Including Exchange and Correlation Effects," *Physical Review*, vol. 140, no. 4, pp. 1133–1138, 1965.
- [23] Perdew and K. Schmidt, "Jacob's ladder of density functional approximations for the exchange-correlation energy Jacob's Ladder of Density Functional Approximations for the Exchange-Correlation Energy," *AIP Conf. Proc.*, vol. 577, no. May, pp. 1–20, 2001.
- [24] A. D. Becke, "A new mixing of Hartree-Fock and local density-functional theories," *The Journal of Chemical Physics*, vol. 98, no. 2, pp. 1372–1377, 1993.
- [25] C. Adamo and V. Barone, "Toward reliable density functional methods without adjustable parameters: The PBE0 model," *Journal of Chemical Physics*, vol. 110, no. 13, pp. 6158–6170, 1999.
- [26] M. Shishkin, M. Marsman, and G. Kresse, "Accurate quasiparticle spectra from self-consistent GW calculations with vertex corrections," *Physical Review Letters*, vol. 99, no. 24, pp. 14–17, 2007.
- [27] J. P. Perdew, "Density functional theory and the band gap problem," *International Journal of Quantum Chemistry*, vol. 28, no. 19 S, pp. 497–523, 1985.
- [28] G. Mahan, *Many-Particle Physics*. Springer Science, 2000.
- [29] A. L. Fetter and J. D. Walecka, *Quantum Theory of Many-Particle Systems*. McGRAW-HILL BOOK COMPANY, 1971.
- [30] G. Tirimbò, V. Sundaram, O. Cañizal, W. Scharpach, J. Sijen, C. Junghans, J. Brown, F. Z. Ruiz, N. Renaud, J. Wehner, and B. Baumeier, "Excited-state electronic structure of molecules using many-body Green's functions: Quasiparticles and electron-hole excitations with VOTCA-XTP," *Journal of Chemical Physics*, vol. 152, no. 11, 2020.
- [31] M. Rohlfing and S. G. Louie, "Electron-hole excitations and optical spectra from first principles Michael," *Physical Review B*, vol. 62, no. 8, pp. 1–18, 2000.
- [32] L. Hedin, "New Method for Calculating the One-Particle Green's Function with Application to the Electron-Gas Problem," *Phys. Rev.*, vol. 139, pp. A796—A823, aug 1965.

- [33] P. Rinke, A. Qteish, J. Neugebauer, and M. Scheffler, "Exciting prospects for solids: Exact-exchange based functionals meet quasiparticle energy calculations," *Physica Status Solidi (B) Basic Research*, vol. 245, no. 5, pp. 929–945, 2008.
- [34] M. S. Hybertsen and S. G. Louie, "First-Principles Theory of Quasiparticles: Calculation of Band Gaps in Semiconductors and Insulators," *Phys. Rev. Lett.*, vol. 55, pp. 1418–1421, sep 1985.
- [35] G. Strinati, "Effects of dynamical screening on resonances at inner-shell thresholds in semiconductors," *Physical Review B*, vol. 29, no. 10, pp. 5718–5726, 1984.
- [36] G. Tirimbò, X. De Vries, C. H. Weijtens, P. A. Bobbert, T. Neumann, R. Coehoorn, and B. Baumeier, "Quantitative predictions of photoelectron spectra in amorphous molecular solids from multiscale quasiparticle embedding," *Physical Review B*, vol. 101, no. 3, 2020.
- [37] T. Zuehlsdorff, *Computing the Optical Properties of Large Systems*. Springer International Publishing, 2015.
- [38] C. A. Ullrich and Z. hui Yang, "A Brief Compendium of Time-Dependent Density Functional Theory," *Brazilian Journal of Physics*, vol. 44, no. 1, pp. 154–188, 2014.
- [39] E. Runge and E. K. U. Gross, "Density-Functional Theory for Time-Dependent Systems," *Physical Review Letters*, vol. 52, pp. 997–1000, mar 1984.
- [40] R. Van Leeuwen, "Key concepts in time-dependent density-functional theory," *International Journal of Modern Physics B*, vol. 15, no. 14, pp. 1969–2023, 2001.
- [41] W. G. Schmidt, "Quantum Chemistry," 2016.
- [42] M. E. Casida and M. Huix-Rotllant, "Many-body perturbation theory (MBPT) and time-dependent density-functional theory (TD-DFT): Mbpt insights about what is missing in, and corrections to, the td-dft adiabatic approximation," *Density-Functional Methods for Excited States*, pp. 1–60, 2015.
- [43] M. E. Casida, "Time-Dependent Density Functional Response Theory for Molecules," in *Recent Advances in Density Functional Methods*, vol. 1, pp. 155–192, WORLD SCIENTIFIC, 1995.
- [44] A. Miller and E. Abrahams, "Impurity conduction at low concentrations," *Physical Review*, vol. 120, no. 3, pp. 745–755, 1960.
- [45] R. A. Marcus, "Electron transfer reactions in chemistry. Theory and experiment," *Reviews of Modern Physics*, vol. 65, no. 3, pp. 599–610, 1993.
- [46] N. G. van Kampen, *Stochastic processes in physics and chemistry*. Amsterdam: Elsevier Science Publishers B.V., rev and en ed., 1992.
- [47] V. Capek, "The Generalized Master Equation Approach To The Phonon-Assisted Hopping: I Zero External Field," *Czech; J. Phys. B*, vol. 32, pp. 777–790, 1982.
- [48] I. Kondov and G. Sutmann, *Multiscale Modelling Methods for Applications in Materials Science*. 2013.
- [49] T. Förster, "Zwischenmolekulare Energiewanderung und Fluoreszenz," *Annalen der Physik*, vol. 437, pp. 55–75, jan 1948.
- [50] D. L. Dexter, "A theory of sensitized luminescence in solids," *The Journal of Chemical Physics*, vol. 21, no. 5, pp. 836–850, 1953.

- [51] J. Lee, K. Vandewal, S. R. Yost, M. E. Bahlke, L. Goris, M. A. Baldo, J. V. Manca, and T. V. Voorhis, "Charge transfer state versus hot exciton dissociation in polymer-fullerene blended solar cells," *Journal of the American Chemical Society*, vol. 132, no. 34, pp. 11878–11880, 2010.
- [52] J. Wehner and B. Baumeier, "Multiscale simulations of singlet and triplet exciton dynamics in energetically disordered molecular systems based on many-body Green's functions theory," *New Journal of Physics*, vol. 22, no. 3, 2020.
- [53] M. Pippig and F. Mercuri, "Efficient evaluation of Coulomb interactions in kinetic Monte Carlo simulations of charge transport," *The Journal of Chemical Physics*, vol. 152, no. 16, p. 164102, 2020.
- [54] V. Rühle, A. Lukyanov, F. May, M. Schrader, T. Vehoff, J. Kirkpatrick, B. Baumeier, and D. Andrienko, "Microscopic simulations of charge transport in disordered organic semiconductors," *Journal of Chemical Theory and Computation*, vol. 7, no. 10, pp. 3335–3345, 2011.
- [55] J. Wehner, *Investigation of exciton properties in organic materials via many-body perturbation theory*. PhD thesis, Technische Universiteit Eindhoven, 2019.
- [56] M. J. Abraham, T. Murtola, R. Schulz, S. Páll, J. C. Smith, B. Hess, and E. Lindah, "Gromacs: High performance molecular simulations through multi-level parallelism from laptops to supercomputers," *SoftwareX*, vol. 1-2, pp. 19–25, sep 2015.
- [57] H. Bassler, "Monte Carlo study of dispersive charge-carrier transport in spatially random systems with and without energetic disorder," *Phys. Rev. B*, vol. 35, no. 5, pp. 2295–2302, 1987.
- [58] A. Stone, *The Theory of Intermolecular Forces*. Oxford: Oxford University Press, 2 ed., 2013.
- [59] J. Wehner, L. Brombacher, J. Brown, C. Junghans, O. Çaylak, Y. Khalak, P. Madhikar, G. Tirimò, and B. Baumeier, "Electronic Excitations in Complex Molecular Environments: Many-Body Green's Functions Theory in VOTCA-XTP," *Journal of Chemical Theory and Computation*, vol. 14, no. 12, pp. 6253–6268, 2018.
- [60] V. Rühle, C. Junghans, A. Lukyanov, K. Kremer, and D. Andrienko, "Versatile object-oriented toolkit for coarse-graining applications," *Journal of Chemical Theory and Computation*, vol. 5, no. 12, pp. 3211–3223, 2009.
- [61] J.-L. Bredas, D. Beljonne, V. Coropceanu, and J. Cornil, "Charge-Transfer and Energy-Transfer Processes in  $\pi$ -Conjugated Oligomers and Polymers: A Molecular Picture," *Chemical Reviews*, vol. 104, pp. 4971–5004, nov 2004.
- [62] B. Baumeier, J. Kirkpatrick, and D. Andrienko, "Density-functional based determination of intermolecular charge transfer properties for large-scale morphologies," *Physical Chemistry Chemical Physics*, vol. 12, no. 36, pp. 11103–11113, 2010.
- [63] M. E. Madjet, A. Abdurahman, and T. Renger, "Intermolecular Coulomb Couplings from Ab Initio Electrostatic Potentials: Application to Optical Transitions of Strongly Coupled Pigments in Photosynthetic Antennae and Reaction Centers," *The Journal of Physical Chemistry B*, vol. 110, pp. 17268–17281, aug 2006.
- [64] J. Wehner and B. Baumeier, "Intermolecular Singlet and Triplet Exciton Transfer Integrals from Many-Body Green's Functions Theory," *Journal of Chemical Theory and Computation*, vol. 13, no. 4, pp. 1584–1594, 2017.

- [65] A. Malde, L. Zuo, M. Breeze, M. Stroet, D. Poger, P. Nair, C. Oostenbrink, and A. Mark, "An Automated force field Topology Builder (ATB) and repository: version 1.0.," *Journal of Chemical Theory and Computation*, vol. 7, pp. 4026–4037, 2011.
- [66] M. Stroet, B. Caron, K. M. Visscher, D. P. Geerke, A. K. Malde, and A. E. Mark, "Automated Topology Builder Version 3.0: Prediction of Solvation Free Enthalpies in Water and Hexane," *Journal of Chemical Theory and Computation*, vol. 14, pp. 5834–5845, nov 2018.
- [67] F. Neese, "The ORCA program system," *WIREs Computational Molecular Science*, vol. 2, pp. 73–78, jan 2012.
- [68] F. Weigend and R. Ahlrichs, "Balanced basis sets of split valence, triple zeta valence and quadruple zeta valence quality for H to Rn: Design and assessment of accuracy," *Physical Chemistry Chemical Physics*, vol. 7, pp. 3297–3305, sep 2005.
- [69] J. J. M. van der Holst, F. W. A. van Oost, R. Coehoorn, and P. A. Bobbert, "Electron-hole recombination in disordered organic semiconductors: Validity of the Langevin formula," *Physical Review B*, vol. 80, p. 235202, dec 2009.
- [70] G. Tirimbò, X. De Vries, C. H. Weijtens, P. A. Bobbert, T. Neumann, R. Coehoorn, and B. Baumeier, "Quantitative predictions of photoelectron spectra in amorphous molecular solids from multiscale quasiparticle embedding," *Physical Review B*, vol. 101, no. 3, pp. 1–10, 2020.
- [71] J. Gärtner and W. König, "The Parabolic Anderson Model," *Interacting Stochastic Systems*, pp. 153–179, 2005.
- [72] C. Cooper, A. Frieze, and T. Radzik, "Multiple Random Walks and Interacting Particle Systems BT - Automata, Languages and Programming," in *International Colloquium on Automata, Languages, and Programming* (S. Albers, A. Marchetti-Spaccamela, Y. Matias, S. Nikolettseas, and W. Thomas, eds.), (Berlin, Heidelberg), pp. 399–410, Springer Berlin Heidelberg, 2009.
- [73] M. Klessinger and J. Michl, *Excited States and Photochemistry of Organic Molecules*. VCH Publishers, Inc, 1995.
- [74] R. Mcweeny and B. T. Sutcliffe, *Methods of molecular quantum mechanics LK - <https://tue.on.worldcat.org/oclc/989652452>*. London SE - XII, 307 p: Academic Press, repr. with ed., 1976.
- [75] Z. G. Yu, D. L. Smith, A. Saxena, R. L. Martin, and A. R. Bishop, "Molecular geometry fluctuations and field-dependent mobility in conjugated polymers," *Physical Review B - Condensed Matter and Materials Physics*, vol. 63, no. 8, pp. 1–9, 2001.
- [76] J. Cottaar, *Modeling of charge-transport processes for predictive simulation of OLEDs*. No. 2012, 2012.
- [77] W. Zhou, C. Zimmermann, and C. Jungemann, "Simulation of bipolar organic semiconductor devices based on the master equation including generation and recombination," *International Conference on Simulation of Semiconductor Processes and Devices, SISPAD*, vol. 2015-October, no. 1, pp. 136–139, 2015.

# Acknowledgements

I would like to thank Jens Wehner for getting me up to speed with C++ programming and his general advice on implementing models and in particular the kinetic Monte Carlo simulator at the start of the project. For his willingness to answer all my short and long questions in the office, I would like to thank Gianluca Tirimbo. He has spend hours and sometimes complete afternoons helping me understand physical and computational concepts necessary for the project. I would also like to thank the Baumeier research group in general for their work on the VOTCA-XTP package on which this project heavily relies.

I am thankful to my parents for their support and the fact that they provided me with the working environment in which I could finish my master thesis in times of the corona virus.

Lastly and most importantly I would like to thank Björn Baumeier. I would like to thank him for giving me the opportunity to work on a project that combines two of my main interests mathematics and chemistry and for his guidance during the project. During the talks in his office or later via video calls he was always able to inspire me and help me to develop my knowledge in the field of computational chemistry. I would also like to thank him for the critical reading of my thesis and his constructive comments that helped to improve the thesis.